3.1 Introduction

A majority of the manufacturing methods to produce complex, near-net shape components are based on either solid or liquid state processing methods. Casting is a liquid state processing route and very cost effective. On the other hand, solid-state techniques like forging or extrusion produce wrought components which are superior to castings but manufacturing costs are significantly higher [Czerwinski, 2006]. Brabazon et al. [Brabazon et al. 2002] reported that conventional casting may result in internal structure defects like oxide and gas entrapment, shrinkage porosity which lead to poor mechanical properties. In the recent past, new techniques are emerging which combine the advantages of these two methods of near net shape production. Semi-solid process is one such process which combines the advantages of casting and forging [Flemings, 1991, Kirkwood, 1994 and Fan, 2002]. For instance, Aluminum alloys which were produced by semi-solid processing became popular due to the accompanying advantages of this process in terms of (a) improved die life due to reduced thermal shocks, (b) relatively better surface finish of the products, (c) negligible liquidus shrinkage because semi-solid laminar flow, (d) ability to produce thin and complex shapes with less shrinkage and porosity [Kirkwood, 1994, Fan, 2002, Boostani and Tahamtan, 2009, omar et al.2005 and Atkinson, 2005]. This method is also utilized for manufacturing automotive, aeronautical and electronic machine tool components. These advantages have been instrumental in rapid replacement of conventionally produced components with ones processed by this semi-solid processing route. One of the chief reasons for the improved properties of the semi-solid process is the formation of globular morphology of the primary phase. Spencer [Spencer, 1971] has observed that non-dendritic solid particles in a liquid matrix due to applying the external force during solidification of Sn-Pb alloy. There are two casting technologies, namely, thixocasting and rheocasting have been developed in semi-

solid processing to produce metallic components. The process of rheocasting involves vigorous melt shearing either during solidification or isothermally with a specific fraction of solid (30 to 65 % solid), followed by pouring or injecting the slurry directly into the die [Mehrabian et al.1972]. In contrast, thixocasting process involves (i) casting of slurry as billet with spherical morphology of primary grains (ii) reheating the non-dendritic billets at semi-solid temperature and (iii) forming the material by the die casting process. Typically, Al alloys (2024, 6082 and 7075) are produced by rheocasting with induction stirring method[Curle et al.2010]. During this process the dendritic arms breaks up into small pieces and subsequently agglomerate and sinter to form clusters[[Flemings et al.1991and Doherty et al.1984]. It is also reported that fragments of the dendrites will grow and form spherical morphology during continuous stirring by reducing the surface energy [Vogel et al.1979]. Alternatively, according to Hellawell [Hellawell et al.1996] grain multiplication also possible by remelting of dendrite arms at their roots instead of breaking the dendrites by mechanical force. Whereas, nucleation and separation from the wall is also possible during semi-solid casting for the evolution of primary phases [Reisi et al.2009 and Niroumand et al.2000]. However, rheocasting technique is cost effective and energy efficient than thixocasting so that the slurry can be made at the production site itself and recycling of scrap materials could be possible [Fan et al.2002, Mehrabian et al.1972, Curle et al.2010, Flemings et al.1976 and Haga et al.2002]. It is reported that Al-10Cu alloy has a comparatively long freezing range [Hasen et al.1958]. In our previous work, it was observed that the Al-10Cu alloy which was produced by metal mould casting technique, have shown long freezing temperature and better wear properties upon subjecting to thermal cycling (chapter – 2). Thus, it could be possible to produce the Al-10Cu alloy by rheocasting technique. In addition, the detailed study of tribology and surface topography of Al-10Cu alloys is not readily available in the literature. Therefore,

in the present investigation, Al-10Cu alloys were produced by rheocasting process and the effect of stirring speed on microstructure as well as dry sliding wear behavior has been systematically studied.

3.2 Experimental Details

3.2.1 Preparation of alloy and wear samples

In this study, Al-10Cu alloy with a composition shown in Table 1 was prepared by melting pure Al and Cu in a graphite crucible using an electric resistance furnace. The melt was stirred for homogeneity and poured into a rectangular cross-sectional cast iron mould after degassing with hexachloroethane. Differential scanning calorimetric measurements suggest the solidus and liquidus temperature of the alloy to be 538.5 and 615 °C respectively. The samples were cut into 20×20×12 mm^3 sizes for microscopy and hardness studies, and 50×50×12 mm^3 for wear testing.

Table 3.1: Chemical Composition of Al-10Cu Alloy

Element	Si	Fe	Cu	Mn	Mg	Zn	Pb	Sn	Al
Weight %	0.686	0.615	10.0	0.326	0.082	0.655	0.0190	0.0257	Balance

3.2.2. Rheocasting procedure

The stir casting furnace with bottom pouring arrangement was used in the rheocasting process. After complete melting and degassing of the alloy, the melt was continuously cooled and stirred to bring the temperature of the melt down to 620 °C so that the primary solid fraction (fs) was about 0.36 as calculated from the Al–Cu phase diagram. A graphite stirrer was used to avoid reaction between the metal and the stirrer. Rheocast samples were produced at three different stirring speeds of 400, 800, and 1200 rpm. The liquid melt, which becomes semi-solid slurry, exits from the bottom of the furnace and fills a rectangular cast iron mould preheated to 100 °C.

3.2.3. Metallography and Mechanical Testing

For microstructural analysis, Samples were prepared by standard metallographic techniques. Keller's reagent (1% vol HF, 1.5% vol HCl, 2.5% vol HNO_3 and balance water) was used for etching of the samples and analyzed under a Leitz Metallux-3 optical microscope. Hardness was measured by LECO LV700 Vickers hardness tester on polished samples at a load of 5 kgf. For each sample, an average of minimum five measurements at different locations is reported. An Instron Universal Testing Machine was used to conduct the room temperature tensile tests on samples prepared as per British Standard Specification (BS EN 10002-1:2001). The ultimate tensile strength was reported based on the average of three tests.

3.2.4. Wear Testing

Dry sliding wear tests were performed by DUCOM TR-20 pin-on-disk machine (Bangalore, India). A cylindrical sample of 8 mm in diameter and 30 mm in length is held firmly against a rotating EN31 steel disc of hardness 62 HRC, whose speed can adjusted by regulators. The frictional force is recorded from the digital display attached to the wear testing machine. The cantilever mechanism of the machine applies the predetermined load. The wear testing was conducted at different loads ranging from 10-50 N at a sliding speed of 1.0 m/s to 5.0 m/s and for a total sliding distance of 3000 m. The samples were thoroughly cleaned with acetone and weighed before and after every test up to an accuracy of ±0.1 mg. The volumetric loss was estimated in terms of the weight loss and the density using the Archimedes' principle. The worn surfaces (wear tracks) of the specimens were investigated under SEM (ZEISS Model-EVO 18) to understand the wear mechanism. Three-dimensional profiles and surface roughness were observed by a 3D-profilometer from Rtec instruments to analyze the wear phenomenon.

3.3 Results and Discussion

3.3.1 Microstructural Features

Figure 3.1(a) shows the microstructure of the Al-10Cu alloy produced by conventional metal mould casting technique and this exhibited fully dendritic structure. In contrast, Fig. 3.1(b) displayed fragmented dendrites of the same alloy which was produced by the rheocasting technique at a stirring speed of 400 rpm. Fig. 3.2(a) and 3.2(b) show the microstructure of the rheocast samples produced at stirring speeds of 800 and 1200 rpm respectively. Rheocast of the melt at 1200 rpm shows the near-gloubular morphology of α-primary phase in complete contrast to its fully dendritic structure in as cast alloys. This feature arises due to fragmentation of dendrites and consequent spherodization of debris particles. The average grain size was measured to be 55 µm for the 800 rpm and 30 µm for the 1200 rpm samples respectively (Fig. 3.2). This observation of increased grain refinement with higher stirring speeds can be rationalized by increased fragmentation and uniform distribution of solid particles in the slurry at higher stirring speeds resulting into pronounced decrease in grain size. Similar behavior was also reported for Al-10% Cu, Al-Cu alloys and other alloys [Ichikawa et al.1987, Mirzadeh and Niroumand, 2009, Falak and Niroumand, 2005]. The increased stirring speed enhances the shear force and results in increased fragmentation of initially formed dendrites. Consequently, the rapid penetration of liquid along the dendrite arms cause the formation of the primary particles. In contrast, other authors have reported that the broken dendrite branches are acting as crystal nuclei and gives rise to grain refinement of primary particles [Rahimi et al.2015].

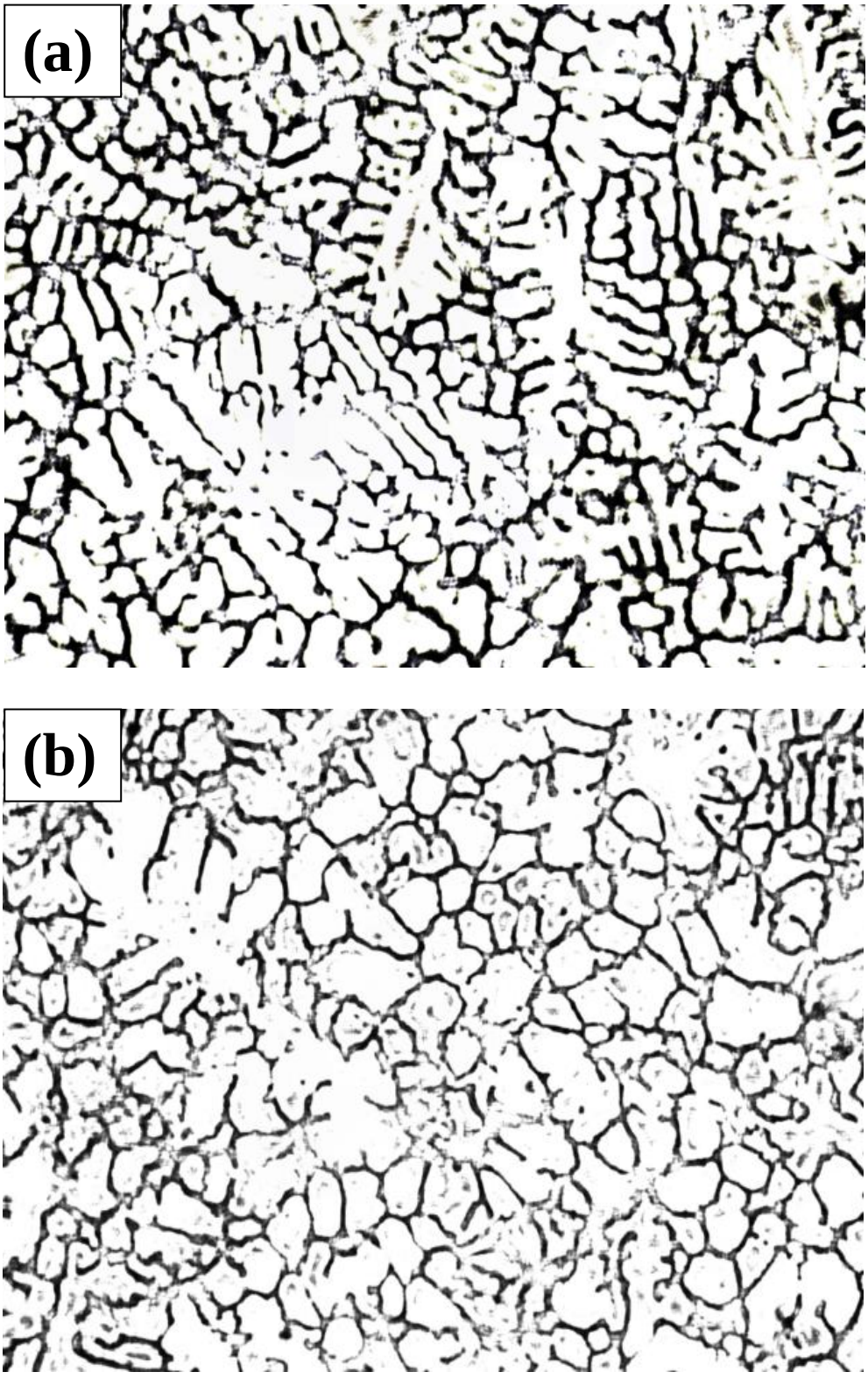

Figure 3.1: Optical micrographs of Al-10Cu alloy produced by (a) metal mould casting and (b) rheocasting at 400 rpm stirring speed.

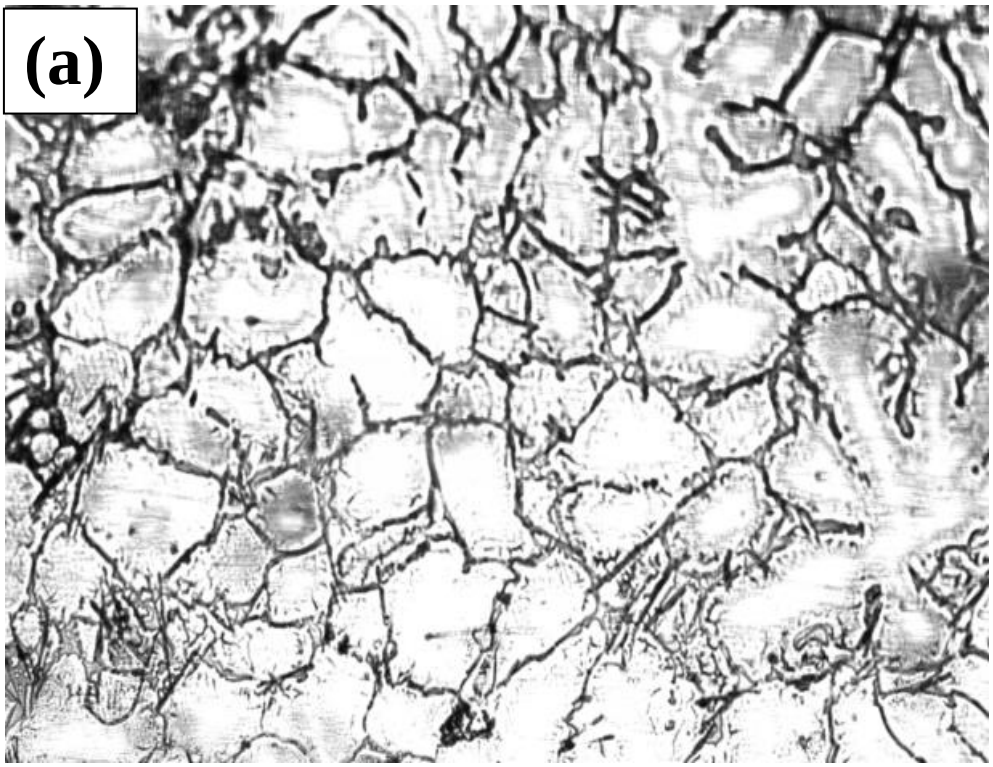
(a)

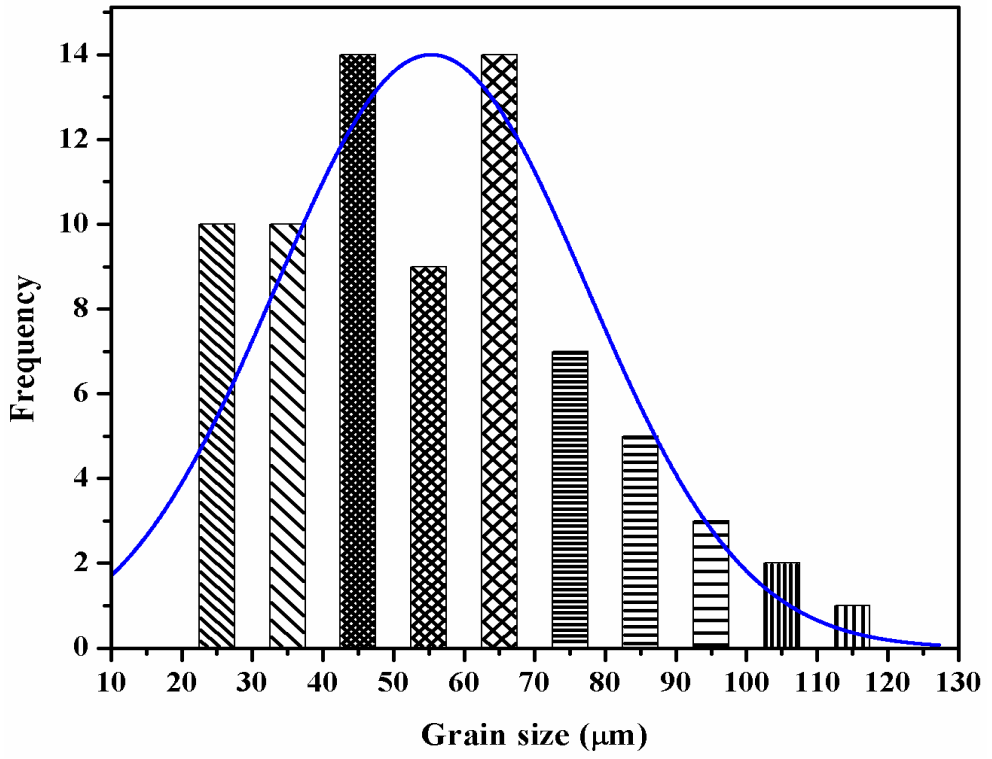
Frequency
0
2
4
6
8
10
12
14
10
20
30
40
50
60
70
80
90
100
110
120
130
Grain size (μm)

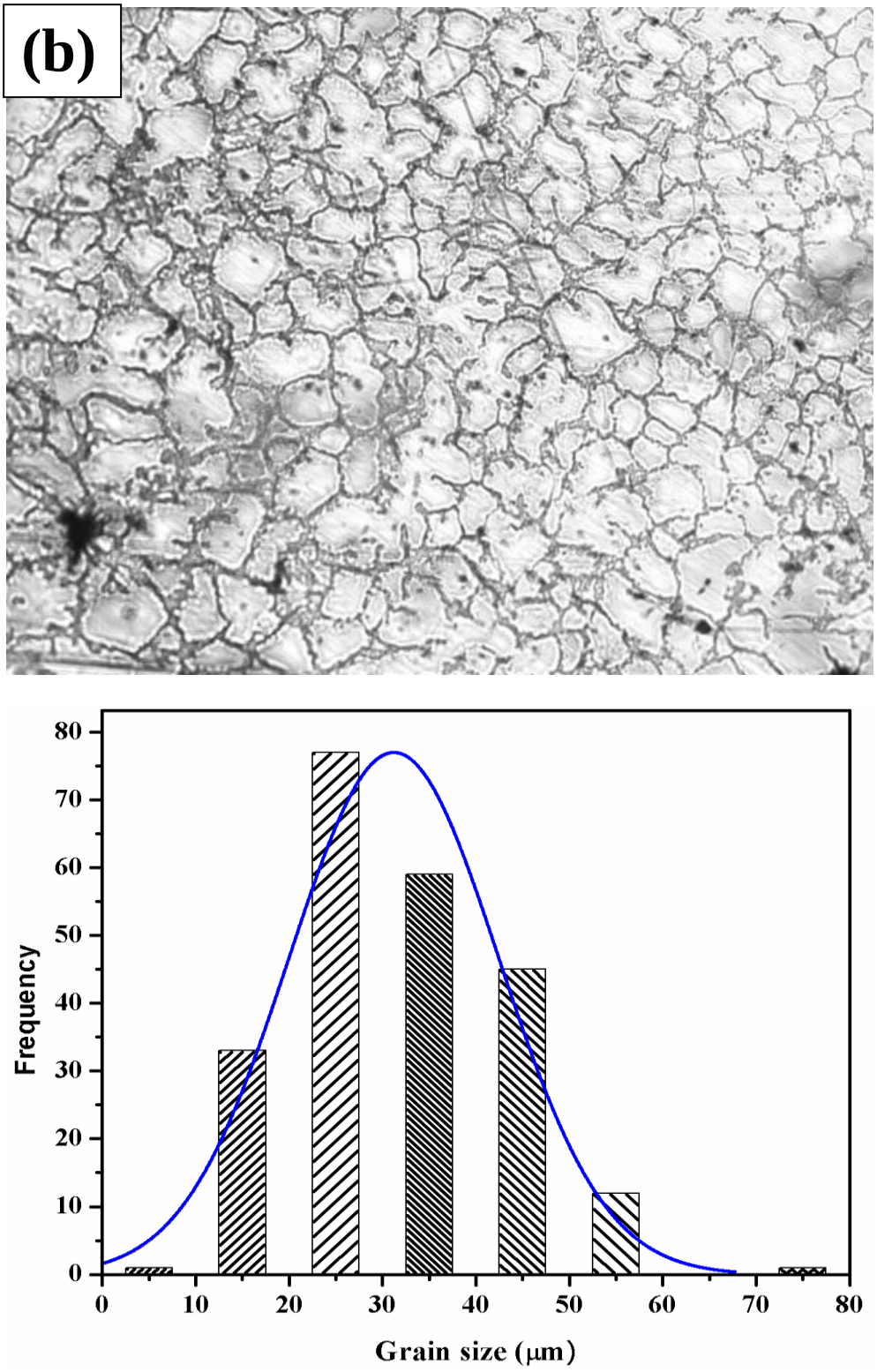

Figure 3.2: Optical micrographs and grain size distribution of Al-10Cu alloy produced by rheocasting method at (a) 800 rpm, (b) 1200 rpm stirring speed.

The SEM micrographs of the rheocastsamples produced at 800 and 1200 rpm were shown in the Figure 3.3. The grain boundary and grain chemistry of the rheocast microstructure is analysed for the 800 rpm and 1200 rpm samples using EDS as shown in Figure 3.4. It can be seen that the Aluminium content in the matrix of the two alloys is higher than that of the grain boundary. In contrast, Copper content is relatively low in the matrix. Based on these observations, it is clear that the grain boundaries are enriched with alloying elements due to solute segregation occurring at high concentrations of Cu and Fe in the inter-dendritic eutectic regions.

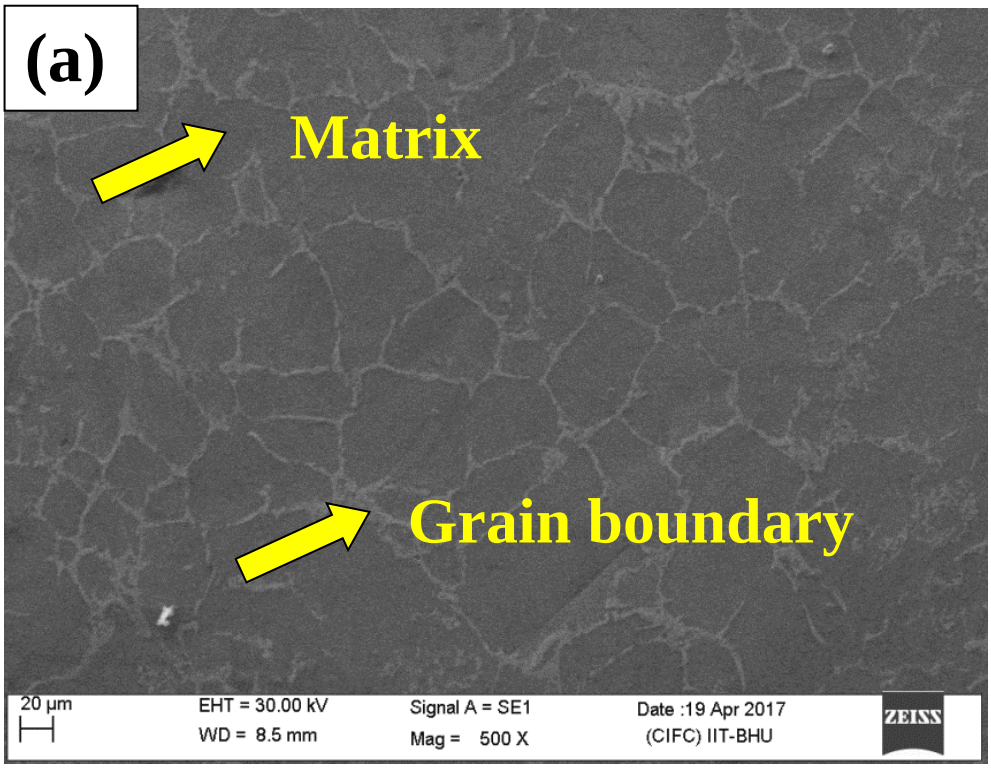

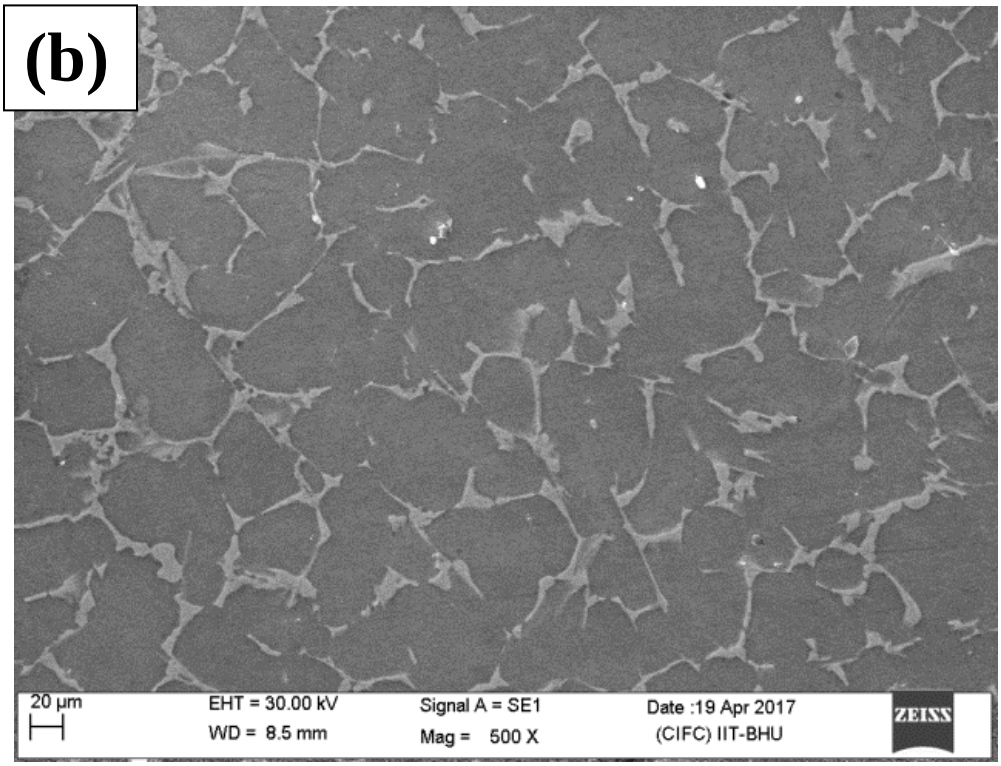

Figure 3.3: SEM micrograph of Al-10Cu alloy produced by rheocasting method at a stirred speed of (a) 800 rpm, (b) 1200 rpm.

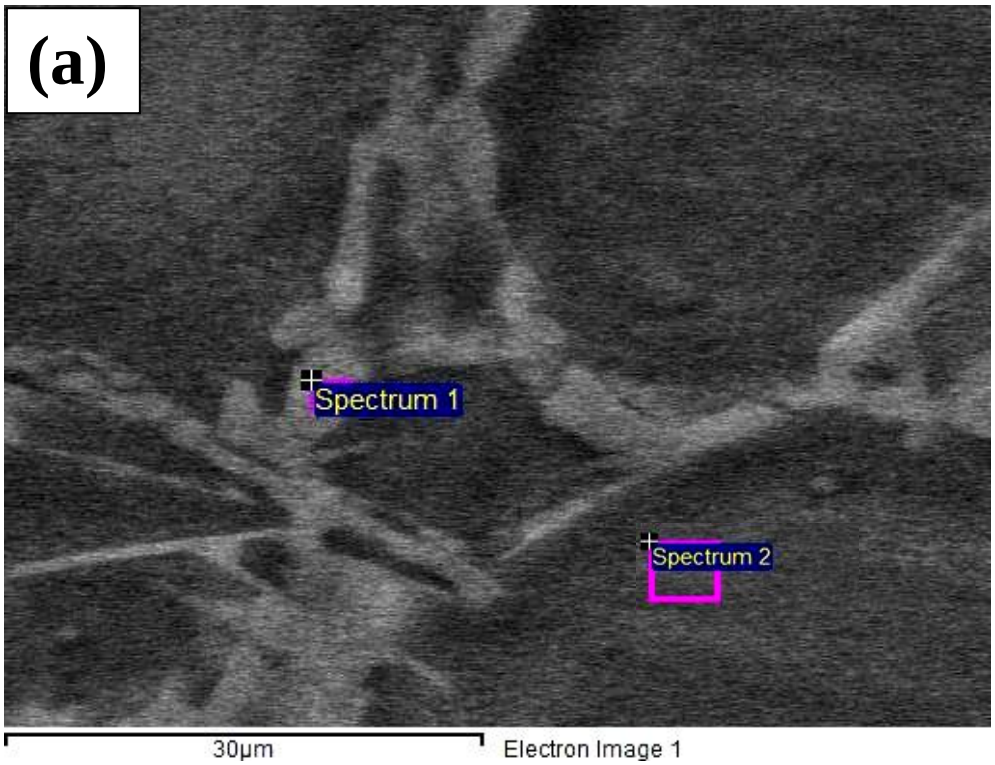

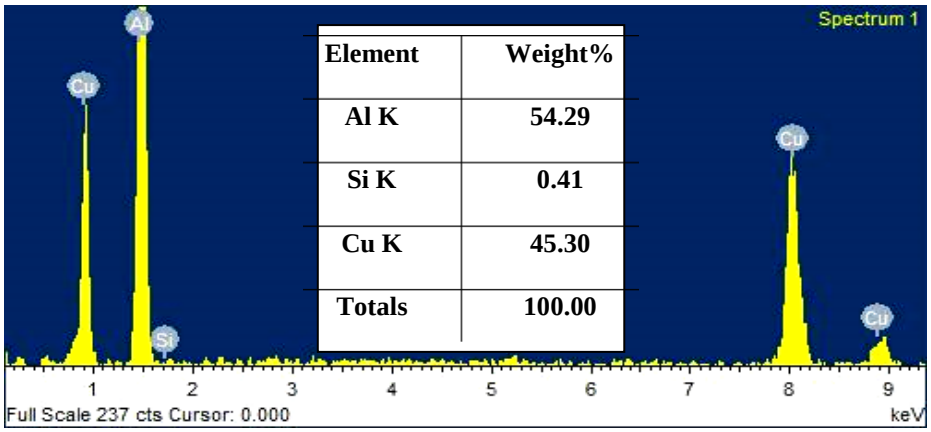

Element	Weight%
Al K	54.29
Si K	0.41
Cu K	45.30
Totals	100.00

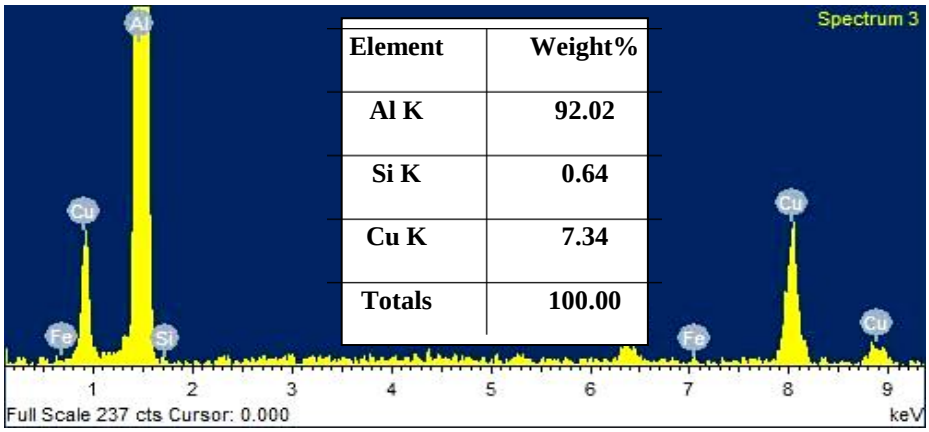

Element	Weight%
Al K	92.02
Si K	0.64
Cu K	7.34
Totals	100.00

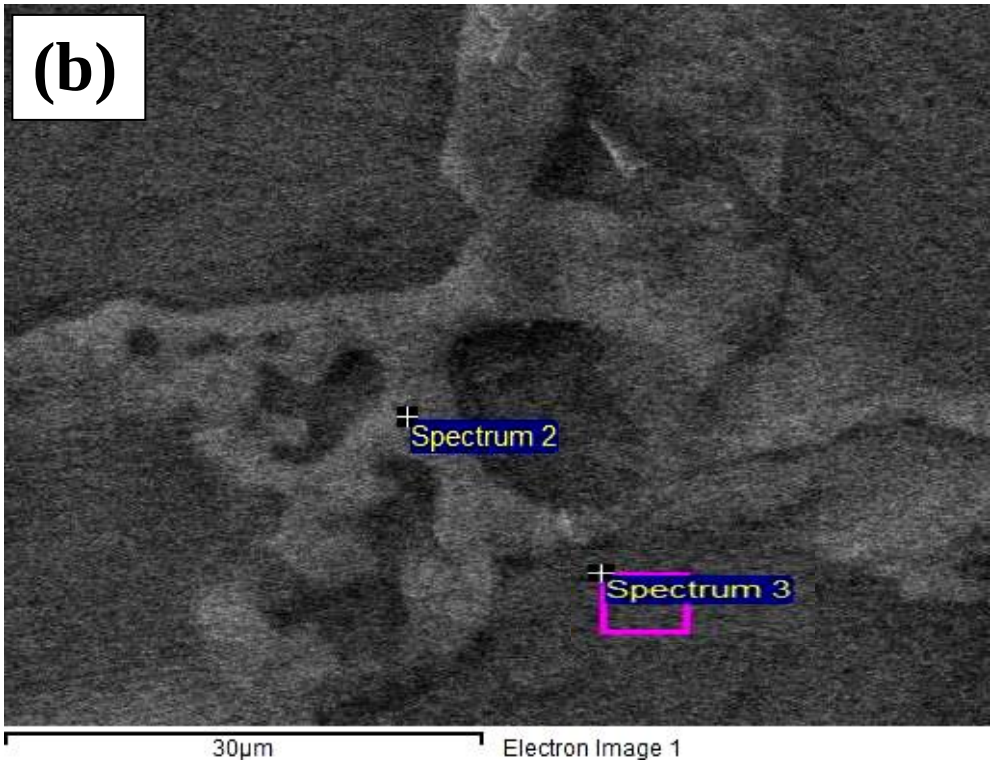

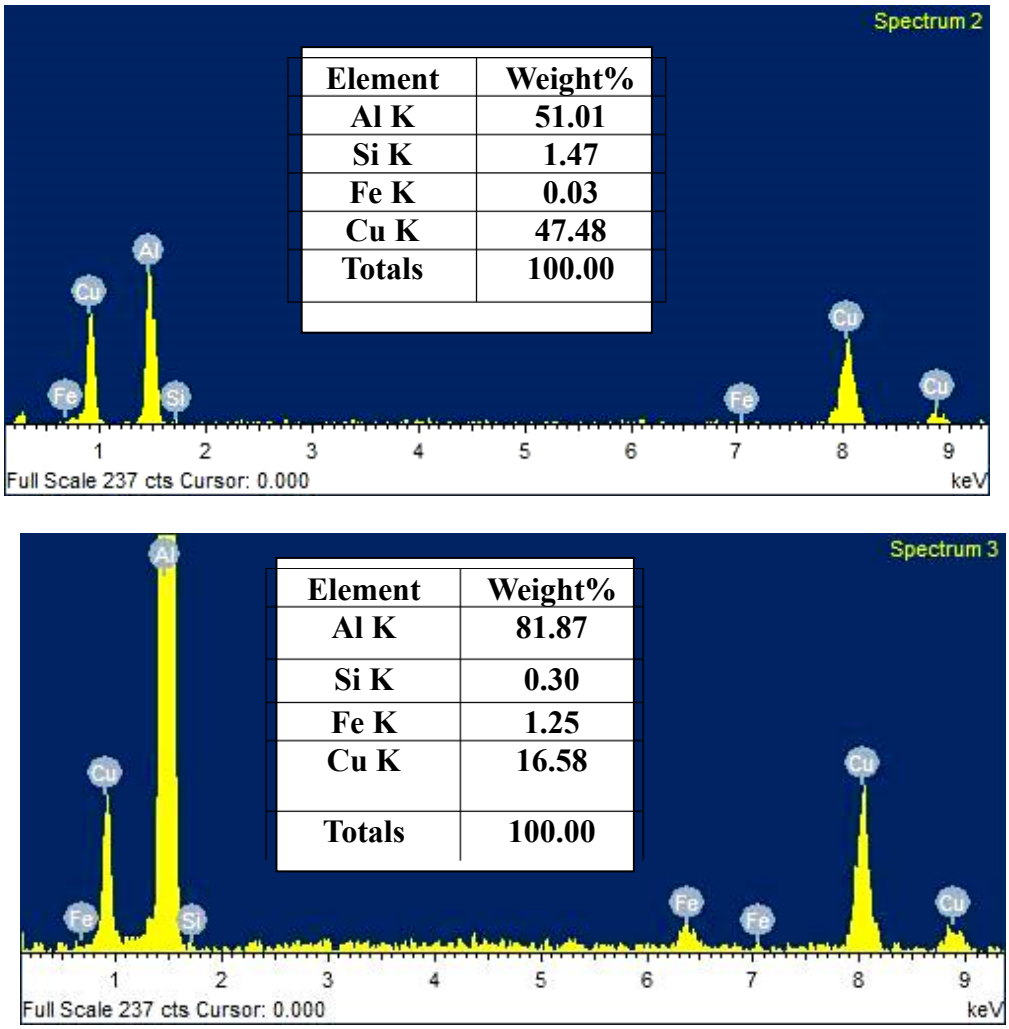

Figure 3.4: EDS analysis results of rheocast alloy at (a) 800 rpm, (b) 1200 rpm.

3.3.2 Mechanical Testing

The microstructural changes are expected to result in variation in the mechanical properties of the alloy. As the stirring speed increased, likeliness for globular grain morphology together with the grain refinement can be expected to enhance the strength of the alloy. Accordingly, Figure 3.5 shows that the hardness and the ultimate tensile strength increased with the stirring speed (with the speed of stirring in the MMC samples being effectively zero). The low hardness value of metal mould cast can be related to the progressive solidification resulting in a dendritic microstructure, while the higher

hardness of the rheocast sample at 1200 rpm is related to the near-globular, fine grain size, as well as to the reduced microporosity.

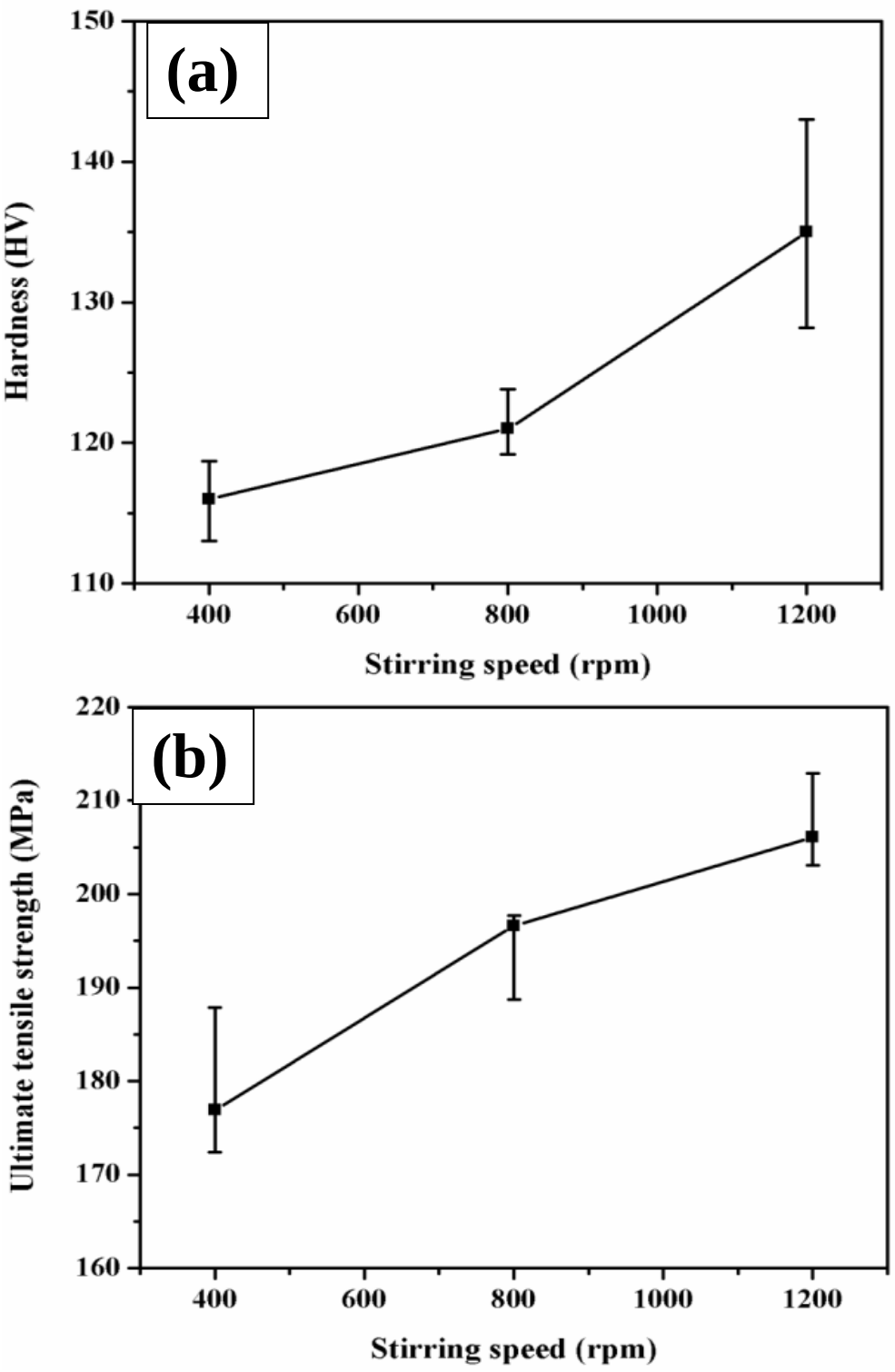

Figure 3.5: Effect of stirring speed on the (a) hardness and (b) ultimate tensile strength of Al-10Cu alloy produced by metal mould casting (MMC) and rheocasting (RC).

3.3.3 Wear Characteristics

The wear characteristics of Al-10Cu alloy produced by metal mould casting and rheocasting at various stirring speeds for a range of applied load 10 N to 50 N shown in the Figures 3.6 to 3.8.

3.3.3.1 Effect of variables

Figure 3.6(a) shows the variation of cumulative volume loss against sliding distance for metal mould cast alloy and rheocast alloy produced at various stirring speeds under constant applied load of 30 N at a constant sliding velocity 1 m/s. Here, the cumulative volume loss is calculated at 1 m/s sliding velocity for total sliding distance 3000 m in intervals of 600 m. It can be seen that, the cumulative volume loss of the alloy produced by rheocasting at 1200 rpm stirring speed is less compared to metal mould cast alloy and other rheocast alloys. This may be due to microstructure of near globular morphology and fine grain size of the primary phase α at higher speed rheocast. On the other hand, the cumulative volume loss of the Al-10Cu cast alloy is increasing with increasing sliding distance for all samples. It could be due to the standard wear law and similar behavior was also reported [Anasyida et al.2009].

Figure 3.6(b) shows the cumulative volume loss against load for Al-10Cu alloy casts under a constant sliding velocity (1 m/s). From the figure it can be noted that cumulative volume loss increases with increasing load in all the cases. However the cumulative volume loss of rheocast sample produced at 1200 rpm is less compared to other samples. The cumulative volume loss as a function of varying sliding velocity (1 m/s to 5 m/s) under a constant load of 30 N and at a constant sliding distance of 3000 m is shown in the figure 3.6(c). All the samples show lower cumulative volume loss upto sliding velocity of 3m/s. Beyond this speed, slope of wear curve drastically increased for

metal mould cast alloy. The velocity at which the wear mechanism changed from mild to severe is called critical velocity. But in the case of rheocasting under similar tested conditions, the mild wear conditions are continued up to 4 m/s this may be due non-dendritic structure produced through rheocasting process. However the cumulative volume loss of 1200 rpm stirring speed rheocast alloy is less compared to other rheocast samples at lower stirring speeds.

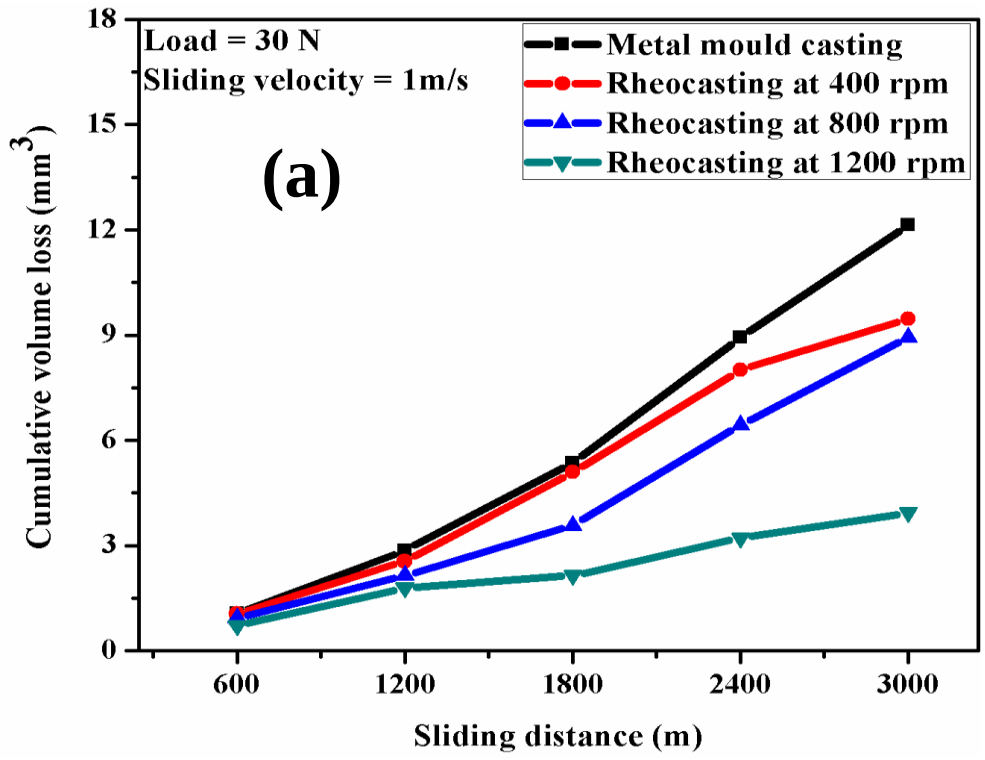

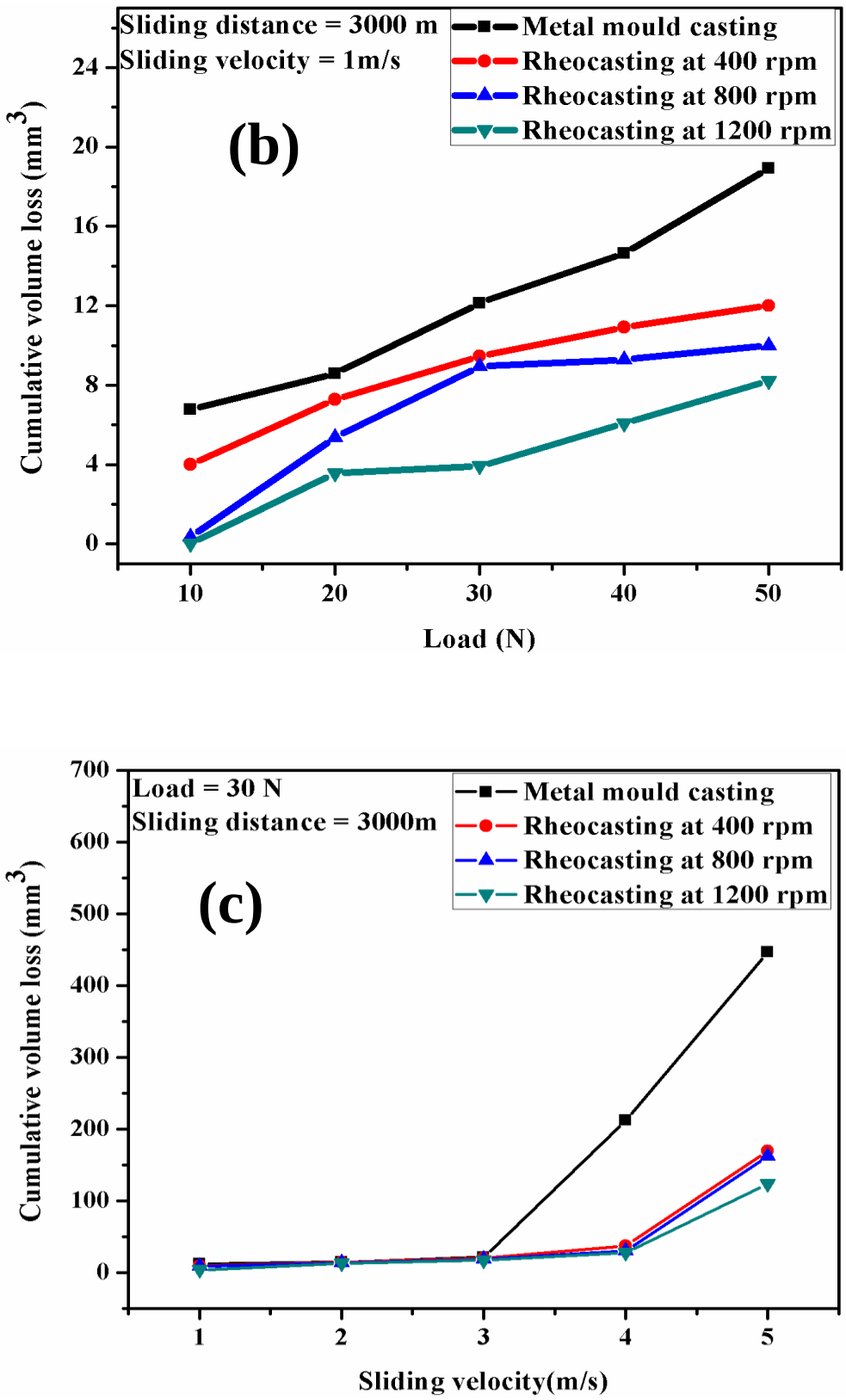

Figure 3.6: The variation in cumulative volume of the samples produced by metal mould casting and rheocasting at different stirred speeds with (a) sliding distance (b) load and (c) sliding velocity.

3.3.3.2 Load and sliding velocity

Figure 3.7(a) indicate the increased wear rate of all the samples with increasing with normal load. The alloy which was produced by rheocasting at 1200 rpm stirring have shown dominant wear rate in comparison to other samples. The rise in bulk temperature and surface contact of the sample at higher loads result in softening the matrix. This leads to enhanced wear rate with increased load. Figure 3.7(b) shows the effect of sliding velocity on the wear rate under a constant load of 30 N. It has been noted that critical velocity for rheocast samples is 4 m/s whereas 3 m/s for metal mould cast alloy. The microstructural change, particularly, finer grain size and its nearly globular morphology of the primary α – phase could be the reasons for the improvement in wear properties of the rheocast alloys.

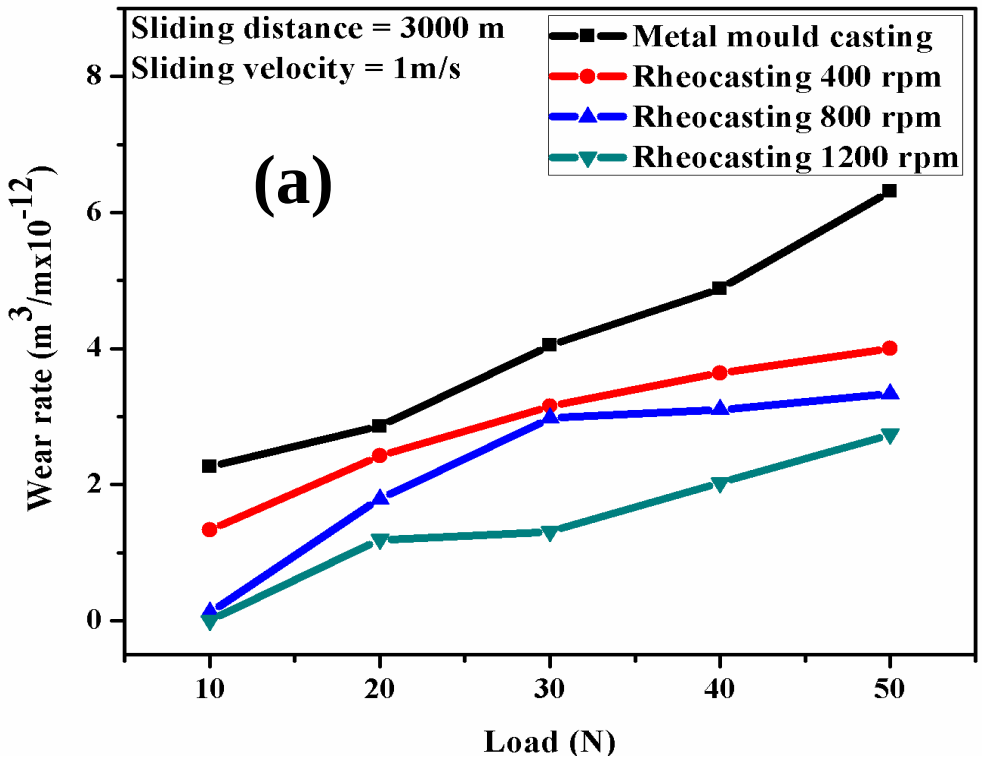

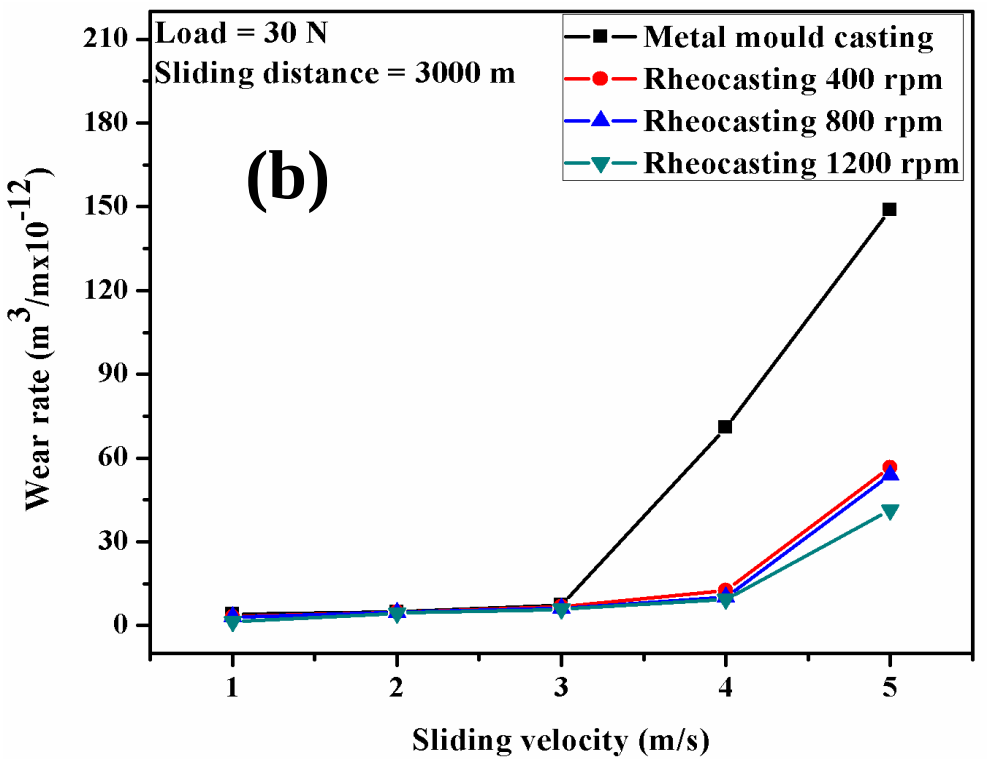

Figure 3.7: The variation in wear rate of metal mould cast and rheocast alloys with (a) load and (b) sliding velocity.

The variation in the coefficient of friction plotted as a function of applied load at a constant sliding velocity (1 m/s) is shown in Figure 3.8(a). The decreased trend in coefficient of friction with an increase in the load was noticed. The coefficient of friction of rheocast alloy produced at 1200 rpm is relatively low at all the loads. For all the samples, coefficient friction is decreasing with load and similar finding was reported elsewhere [Thuong et al.2015]. The locking of asperities could elude the true contact between the wear pin surface and the wear disc at lower loads. This may be the reason for getting high coefficient of friction at lower load [Srivastava et al.2009].

It is well known that the coefficient of friction depends on the material properties like hardness, ultimate tensile strength [Mandal et al.2002]. At higher load, the coefficient of friction has decreased to a low value due to decreased shear strength and this trend was observed for all the samples. The formation of a very fine molten layer at

asperities interactions could also be the reason for reduced values of coefficient of friction.

The low coefficient of friction values were observed in rheocast alloy of 1200 rpm compared to other samples. The variation in the coefficient of friction of the samples plotted as a function of sliding velocity at a load of 30 N is shown in the figure 3.8(b). The coefficient of friction of the samples displayed increasing trend with increase in sliding velocity. However, the coefficient of friction values are relatively less in the 1200 rpm stirred rheocast alloy.

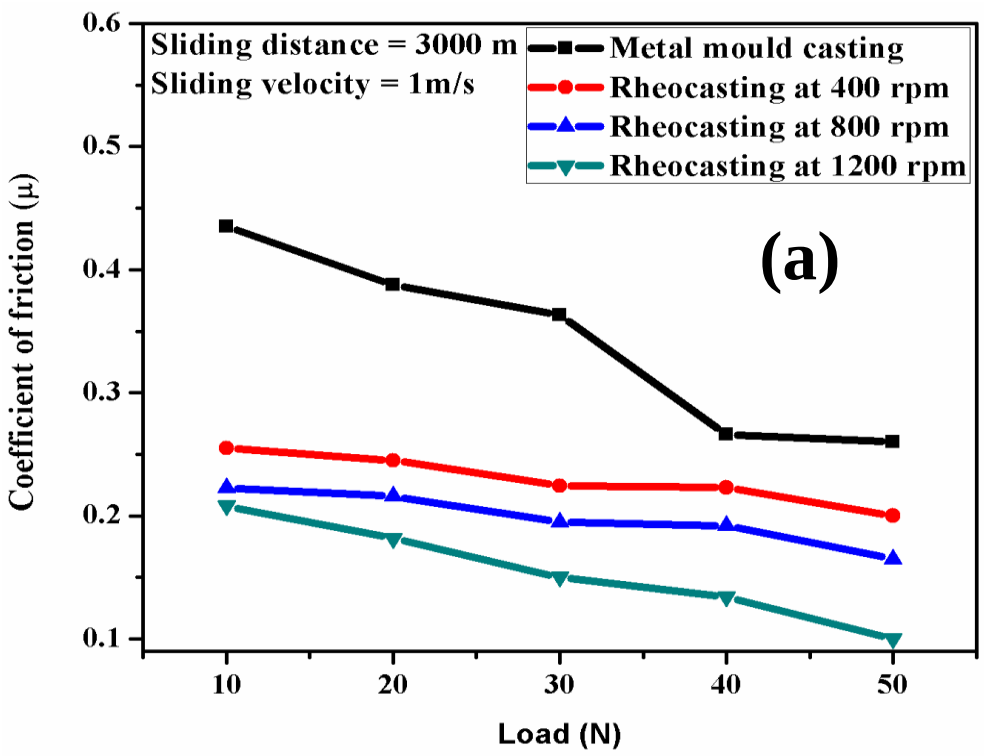

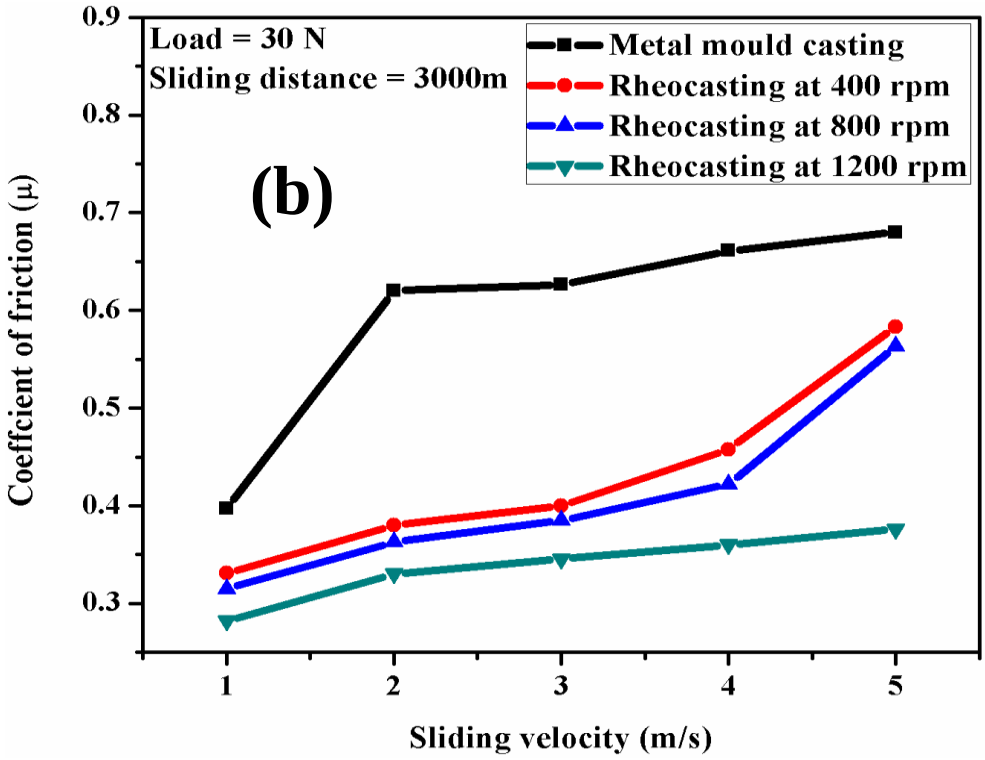

Figure 3.8: The variation in coefficient of friction of metal mould cast and rheocast alloys with (a) load and (b) sliding velocity.

3.3.3.3 Morphology Of Worn-Out Surfaces

The worn surfaces of the wear pins were observed under SEM for understanding the wear mechanism. Generally sliding wear occurs due to three body abrasion, locking of surface asperities and their local welding [Rudrakshi et al. 2007]. Figure 3.9(a) shows the morphology of the worn surface of the metal mould cast alloy tested at 30 N load of 1m/s sliding velocity for the total distance of 3000 m. It shows damaged regions (arrow marked) and continuous grooves formation from one end to the other end. Nucleation and propagation of cracks caused the damaged region. The detachment of a portion from top surface also seen in the worn surface of the metal mould cast alloy. This wear is combination of adhesive and delamination mode and which cause the material removal in the form of sheets and left the craters. The scoring of this metal mould cast alloy is relatively higher than that of the rheocast alloys which are tested under similar testing conditions.

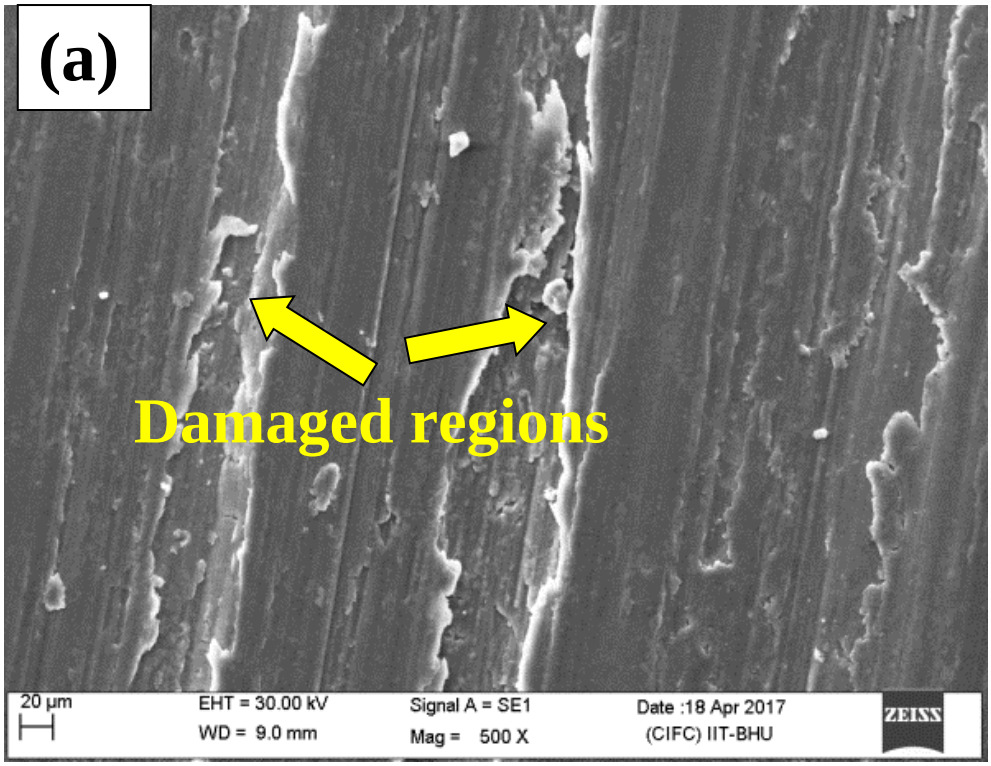
(a)
Damaged regions
20 µm
EHT = 30.00 kV
WD = 9.0 mm
Signal A = SE1
Mag = 500 X
Date :18 Apr 2017
(CIFC) IIT-BHU
ZEISS

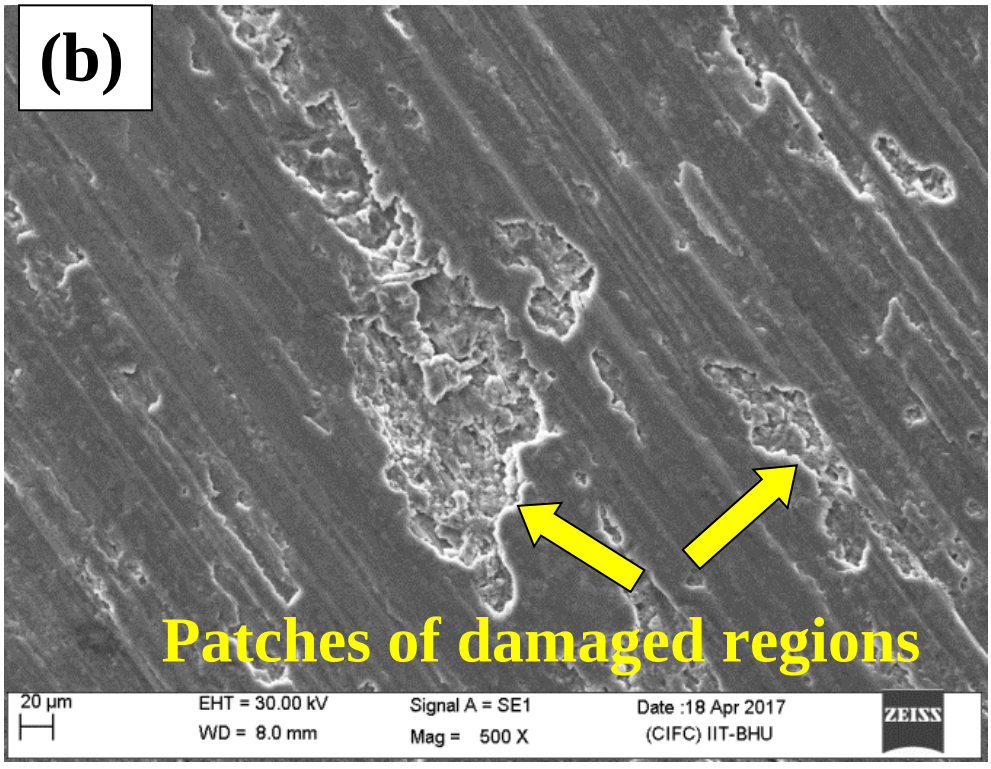
(b)
Patches of damaged regions
20 µm
EHT = 30.00 kV
WD = 8.0 mm
Signal A = SE1
Mag = 500 X
Date :18 Apr 2017
(CIFC) IIT-BHU
ZEISS

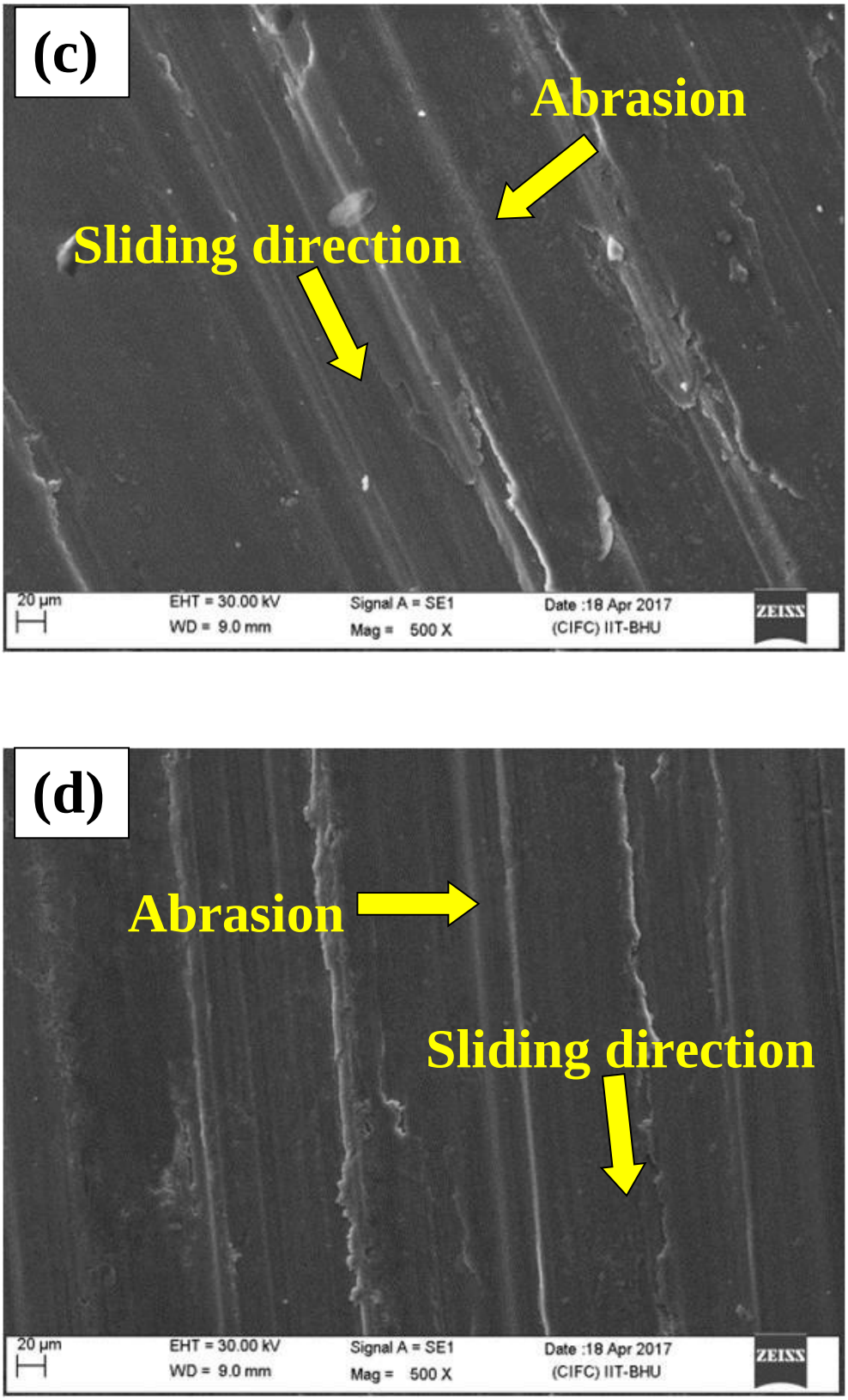

Figure 3.9: SEM micrographs of worn surfaces at 30N load and 1m/s sliding velocity for (a) Metal mould cast alloy (b) 400 rpm (c) 800 rpm and (d) 1200 rpm of rheocast alloys.

Figure 3.9(b) shows the worn surface of the rheocast produced at 400 rpm stirring speed tested at 30 N at a 1m/s sliding velocity and 3000 m sliding distance. The patches of damaged regions and continuous grooves were observed from the end of the surface to the other end. The continuous grooves were observed for rheocast alloys of 800 and 1200 rpm (Figure 3.9 c & d). The ploughing marks were wider with debris particles along the grooves in the case of 800 rpm stirring speed. However ,finer grooves were noticed in 1200 rpm rheocast alloy. This is because of its finer grain size and nearly globular microstructure of the primary α - phase. The amount material removal from finer groove was very small due to abrasion wear [Vencl et al.2014].

Figure 3.10 to 3.12 show the SEM micrographs and EDS analysis of the rheocast alloys produced at 1200, 800 and 400 rpm stirring speed at 5 m/s sliding velocity at a constant load of 30 N. The EDS analysis confirms the presence of oxygen and iron. It indicates the oxidative-metallic wear in the sample. The worn surface of 800 rpm alloy displayed the formation of parallel lips whereas adhesive and delaminated wear was notices for 400 rpm sample.

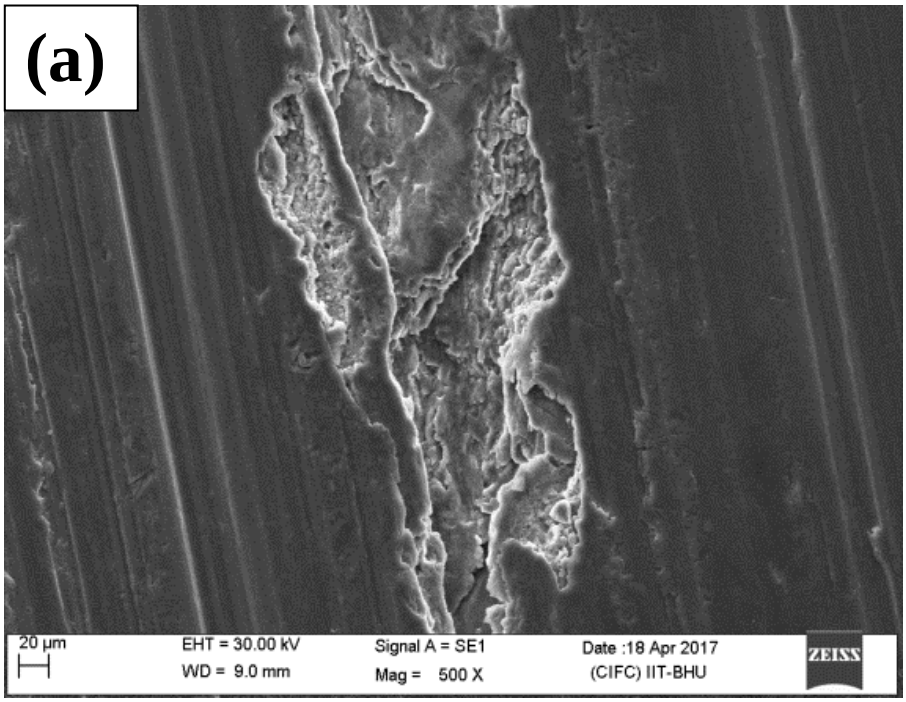

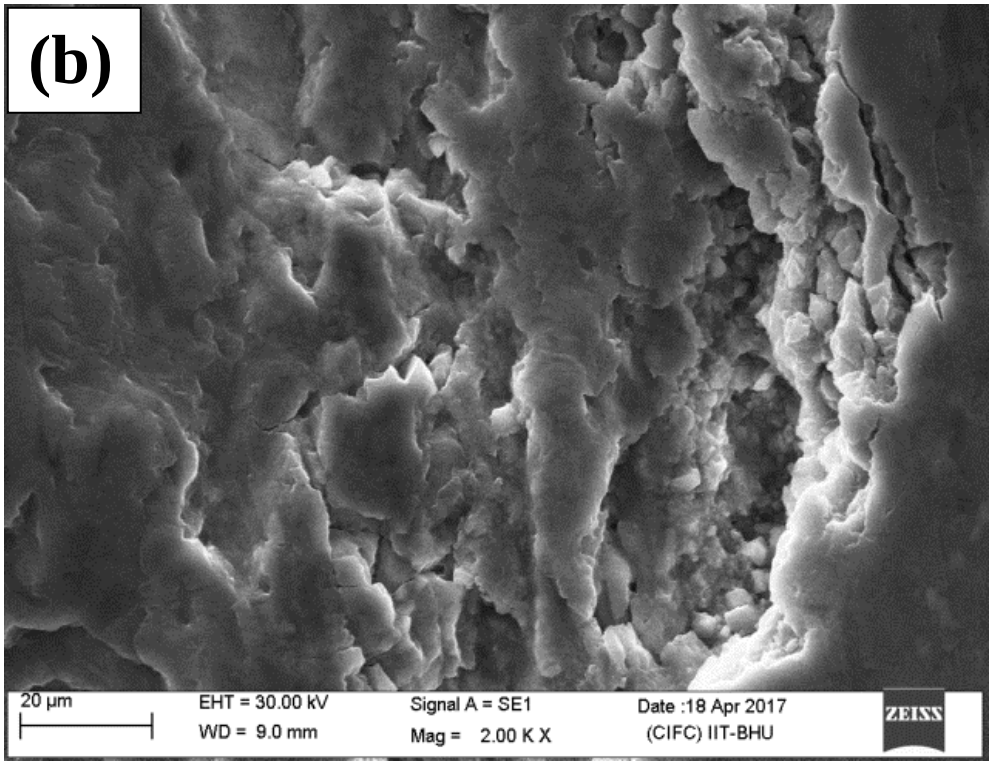

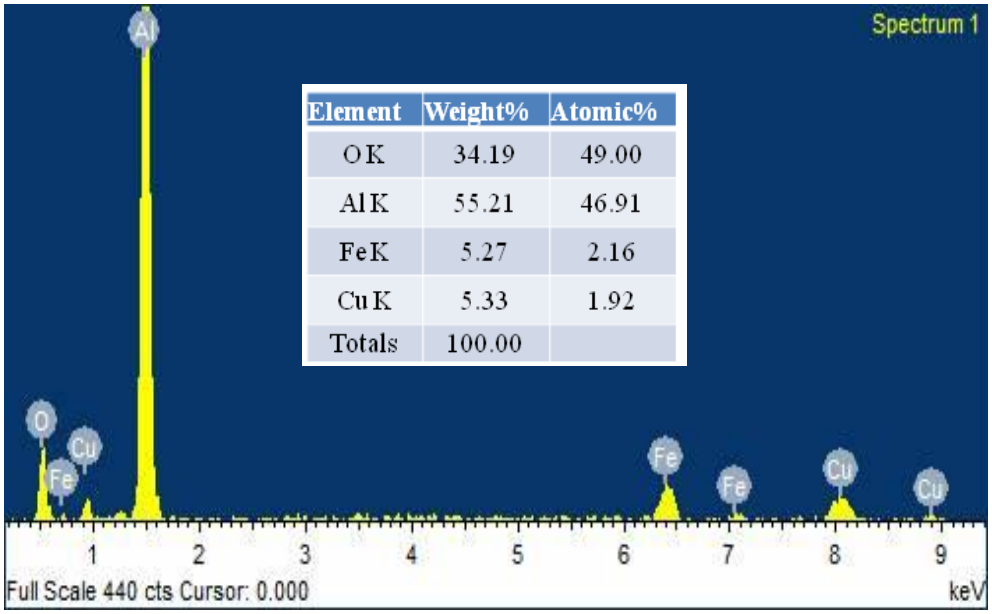

Element	Weight%	Atomic%
O K	34.19	49.00
Al K	55.21	46.91
Fe K	5.27	2.16
Cu K	5.33	1.92
Totals	100.00	

Figure 3.10: SEM micrographs and EDS analysis of 1200 rpm stirring speed rheocast sample worn surfaces tested at 30 N load and 5 m/s sliding velocity at (a) lower and (b) higher magnifications.

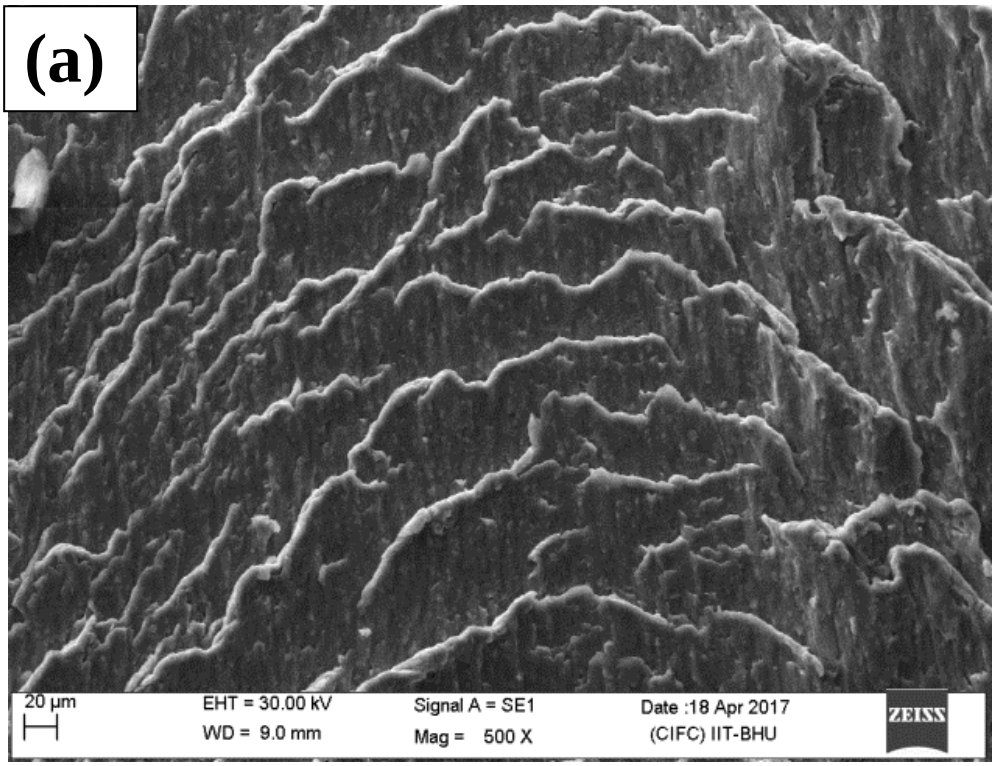
(a)
20 µm
EHT = 30.00 kV
WD = 9.0 mm
Signal A = SE1
Mag = 500 X
Date :18 Apr 2017
(CIFC) IIT-BHU
ZEISS

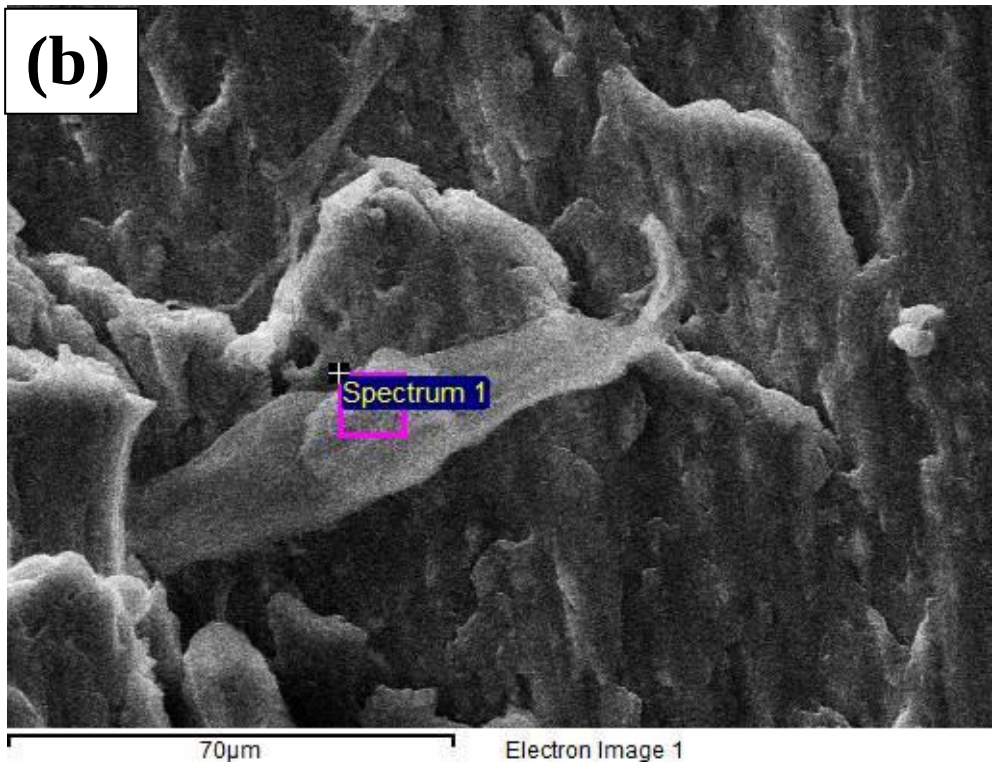
(b)
Spectrum 1
70µm
Electron Image 1

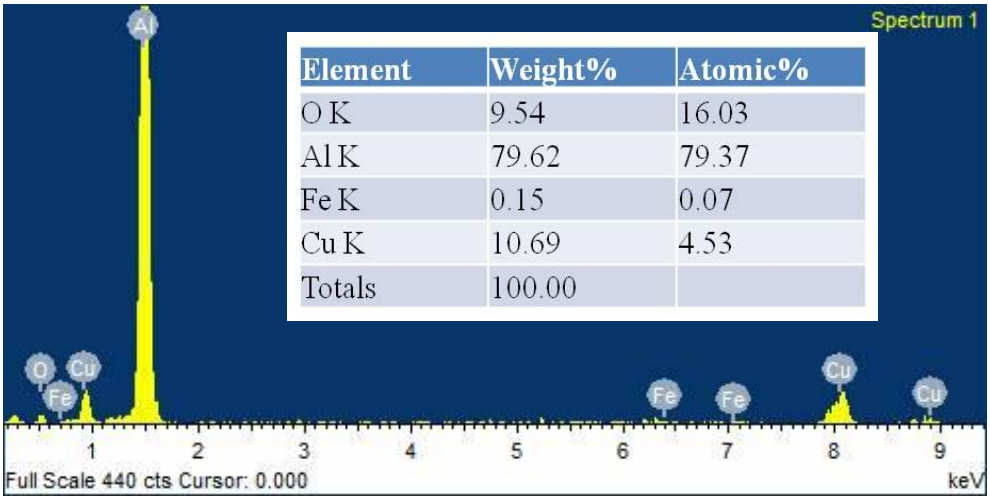

Figure 3.11: SEM micrographs and EDS analysis of 800 rpm stirring speed rheocast sample worn surfaces tested at 30 N load and 5 m/s sliding velocity at (a) lower and (b) higher magnifications.

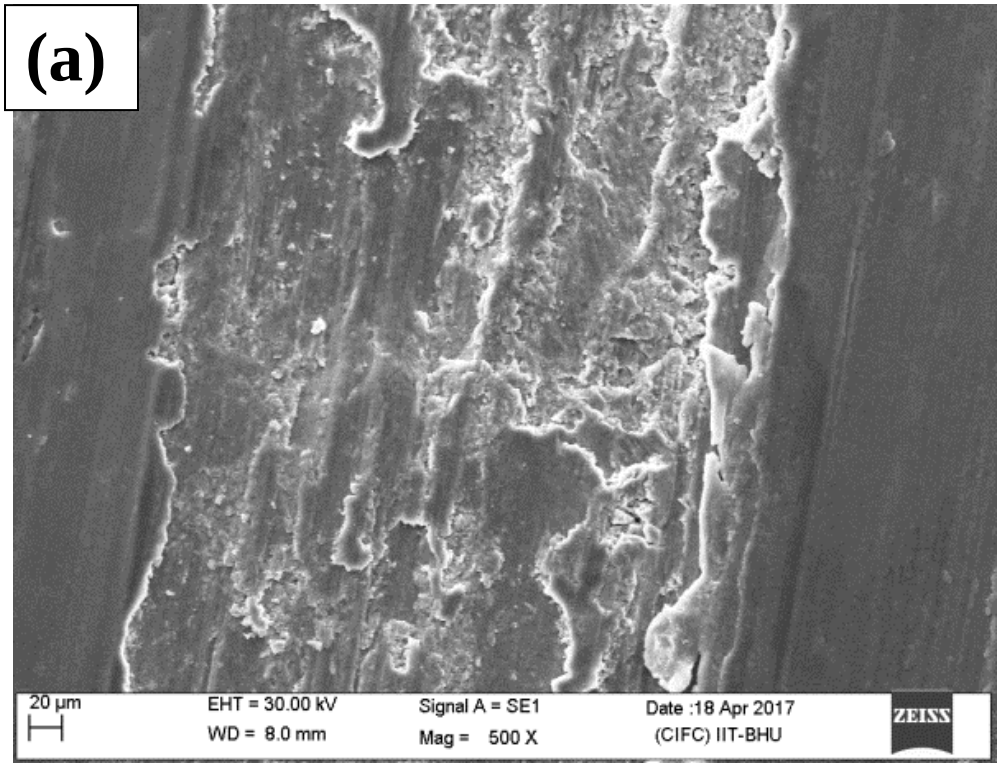

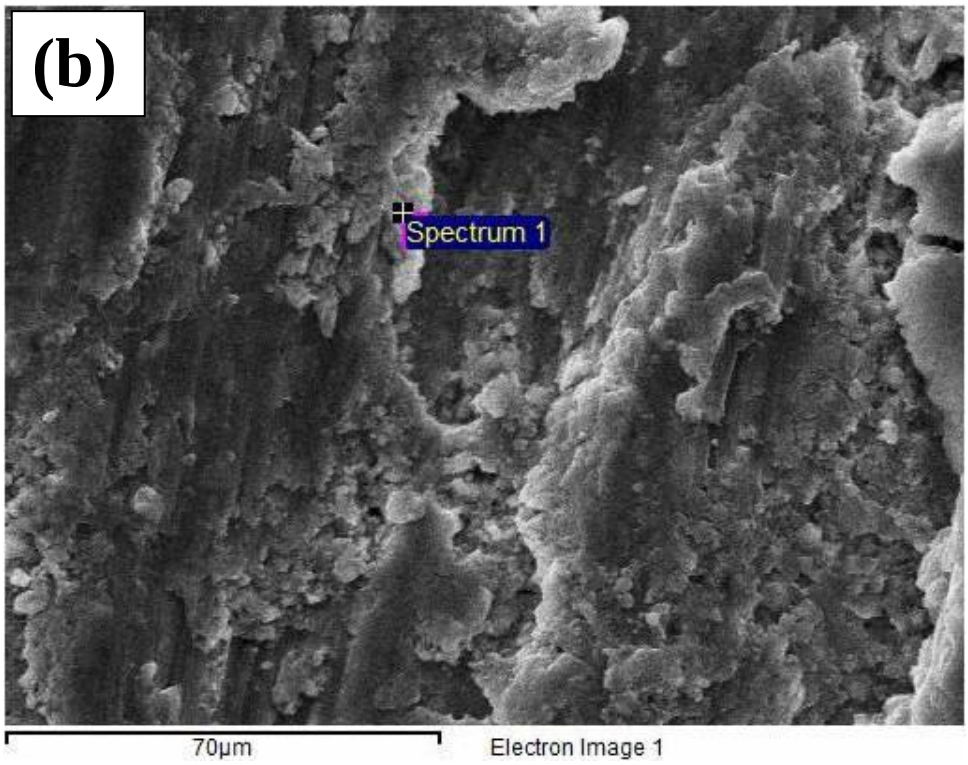

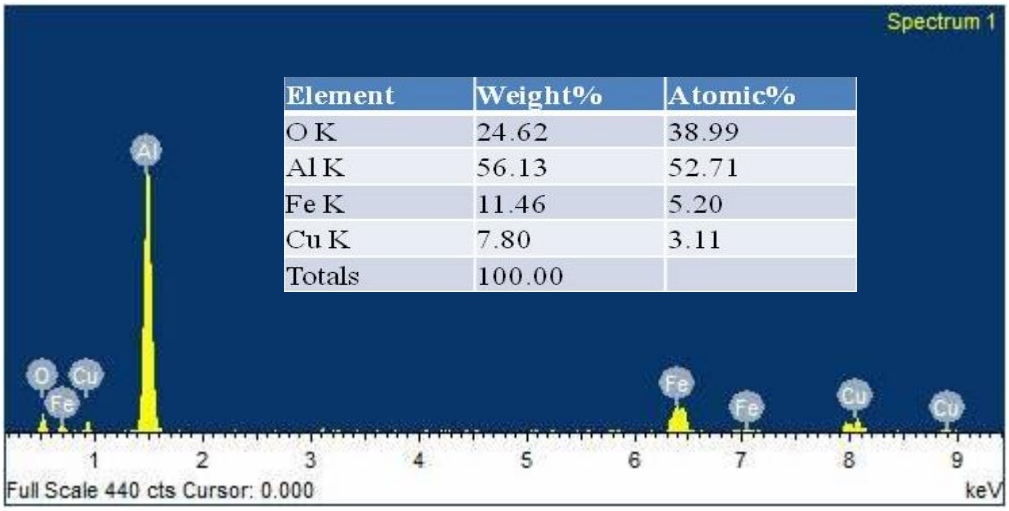

Figure 3.12: SEM micrographs and EDS analysis of 400 rpm stirring speed rheocast sample worn surfaces tested at 30 N load and 5 m/s sliding at (a) lower and (b) higher magnifications.

Figure 3.13 to 3.18 shows the different level of surface roughness and 3D topography produced during wear testing of all the samples. The profiles indicate the variation of surface roughness from valley to peak. To understand the profile nature of the selected area, an average line is drawn in contour which shows the nature of profile on that particular line. The R_a values of the alloys were obtained by 3D–profilometer image and line analysis. Figure 3.13 and 3.14 show the line analysis and 3D-profilometer images of rheocast samples produced at 800 and 1200 rpm stirring speeds load of 50 N and 1 m/s sliding velocity for the 3000 m sliding distance respectively. The R_a value for 1200 rpm alloy is lower than that of 800 rpm sample. Finer grooves were observed from one end to the other end in the both 3D profiles of rheocast samples.

The line analysis and 3D profilometry images for the same samples at load of 30 N and 3 m/s sliding velocity for the 3000 m sliding distance is shown in Figure 3.15 and 3.16. Under these testing conditions, the grooves relatively become wider. Whereas, more deformed surface was observed at a load 30 N but the sliding velocity was increased to 5 m/s for the sliding distance of 3000 m (Figure 3.17 and 3.18).

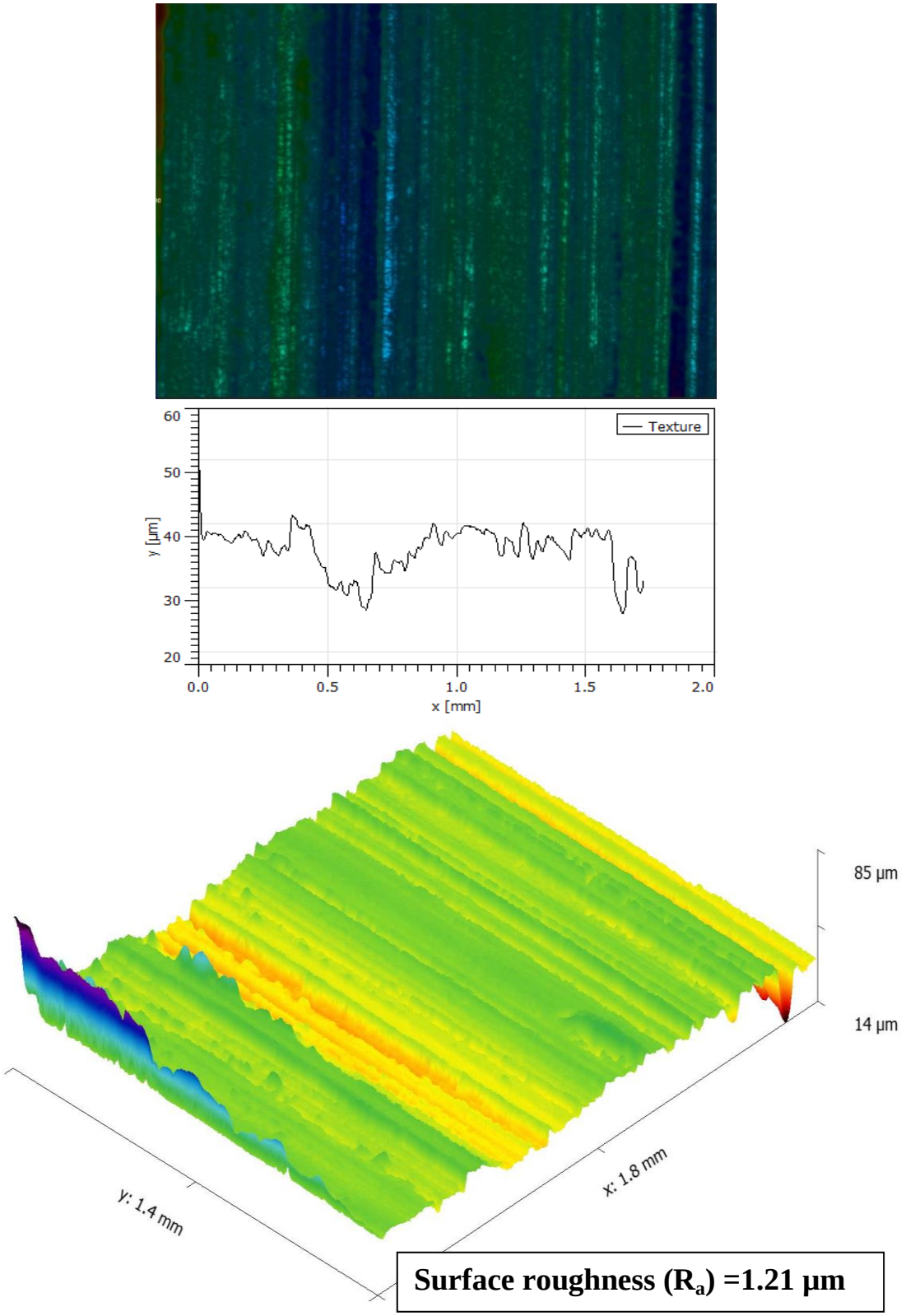

Figure 3.13: Line analysis and 3D profilometer image for rheocast with 800 rpm stirring speed at 50 N load and 1 m/s sliding velocity.

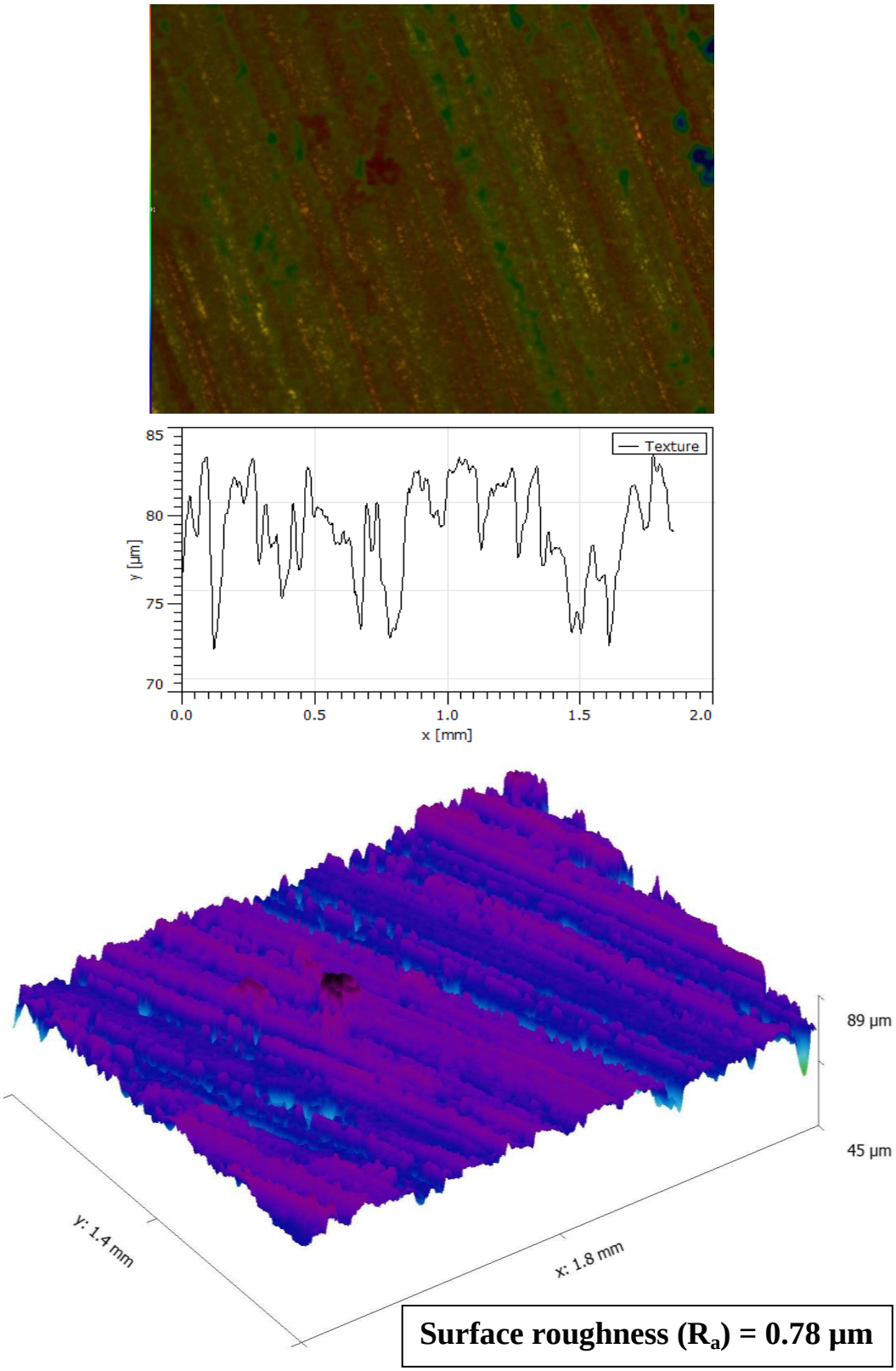

Figure 3.14: Line analysis and 3D profilometer image for rheocast with 1200 rpm stirring speed at 50 N load and 1 m/s sliding velocity.

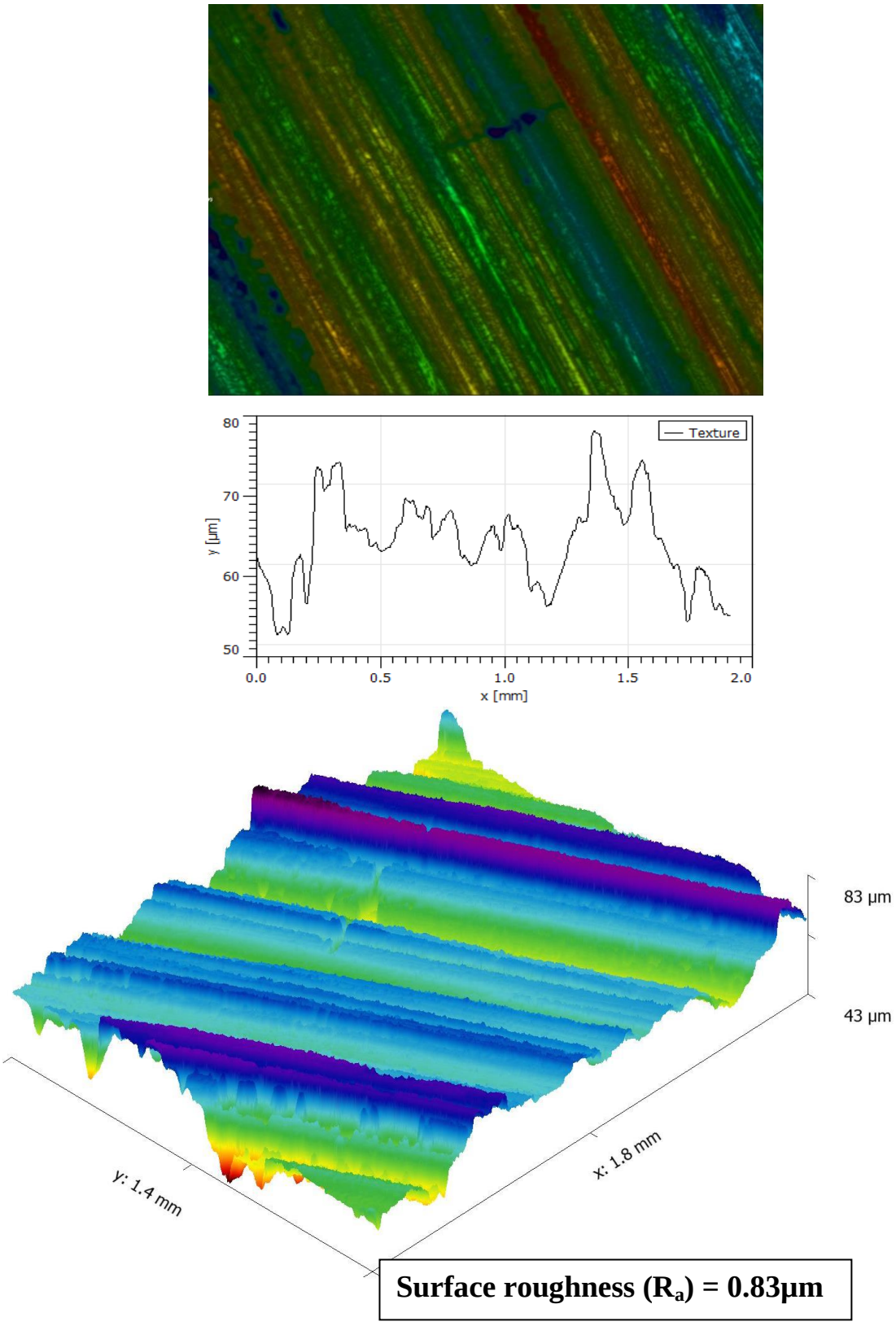

Figure 3.15: Line analysis and 3D profilometer image for the alloy produced by rheocasting with 800 rpm stirring speed at 30 N load and 3 m/s sliding velocity.

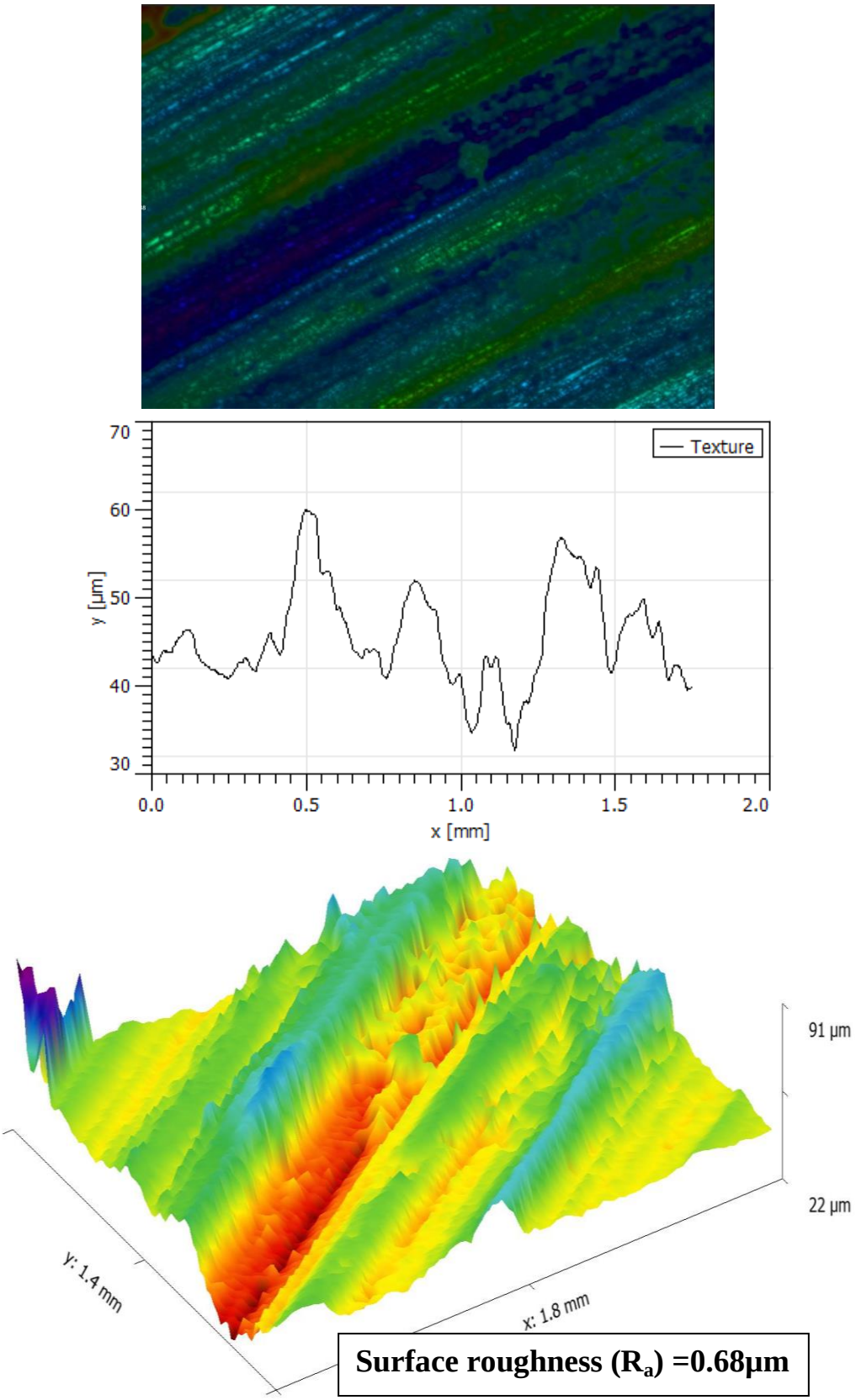

Figure 3.16: Line analysis and 3D profilometer image for rheocast alloy with 1200 rpm stirring speed at 30 N load and 3 m/s sliding velocity.

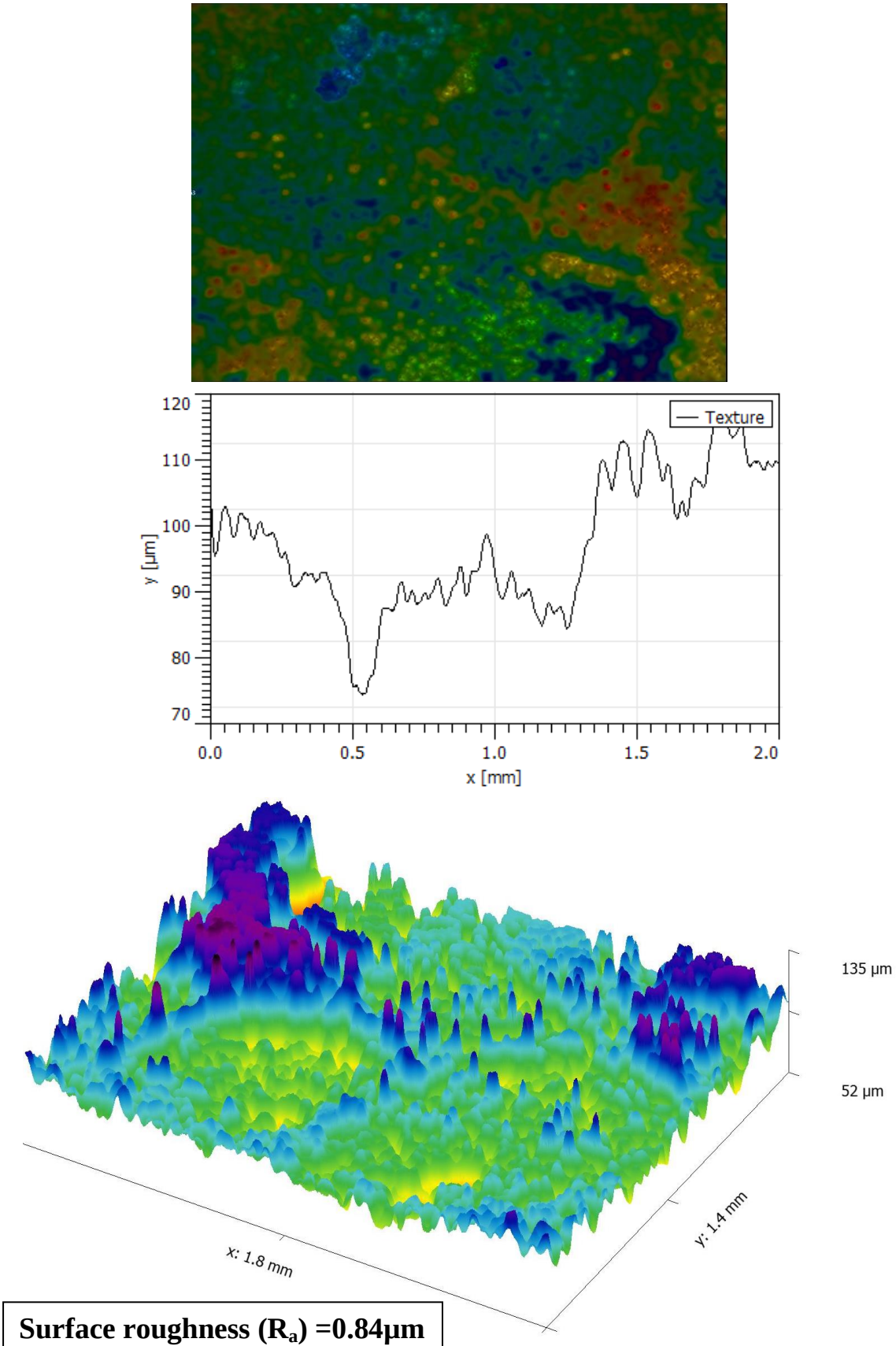

Surface roughness (R_a) =0.84µm

Figure 3.17: Line analysis and 3D profilometer image for the alloy produced by rheocasting with 800 rpm stirring speed at 30 N load and 5 m/s sliding velocity

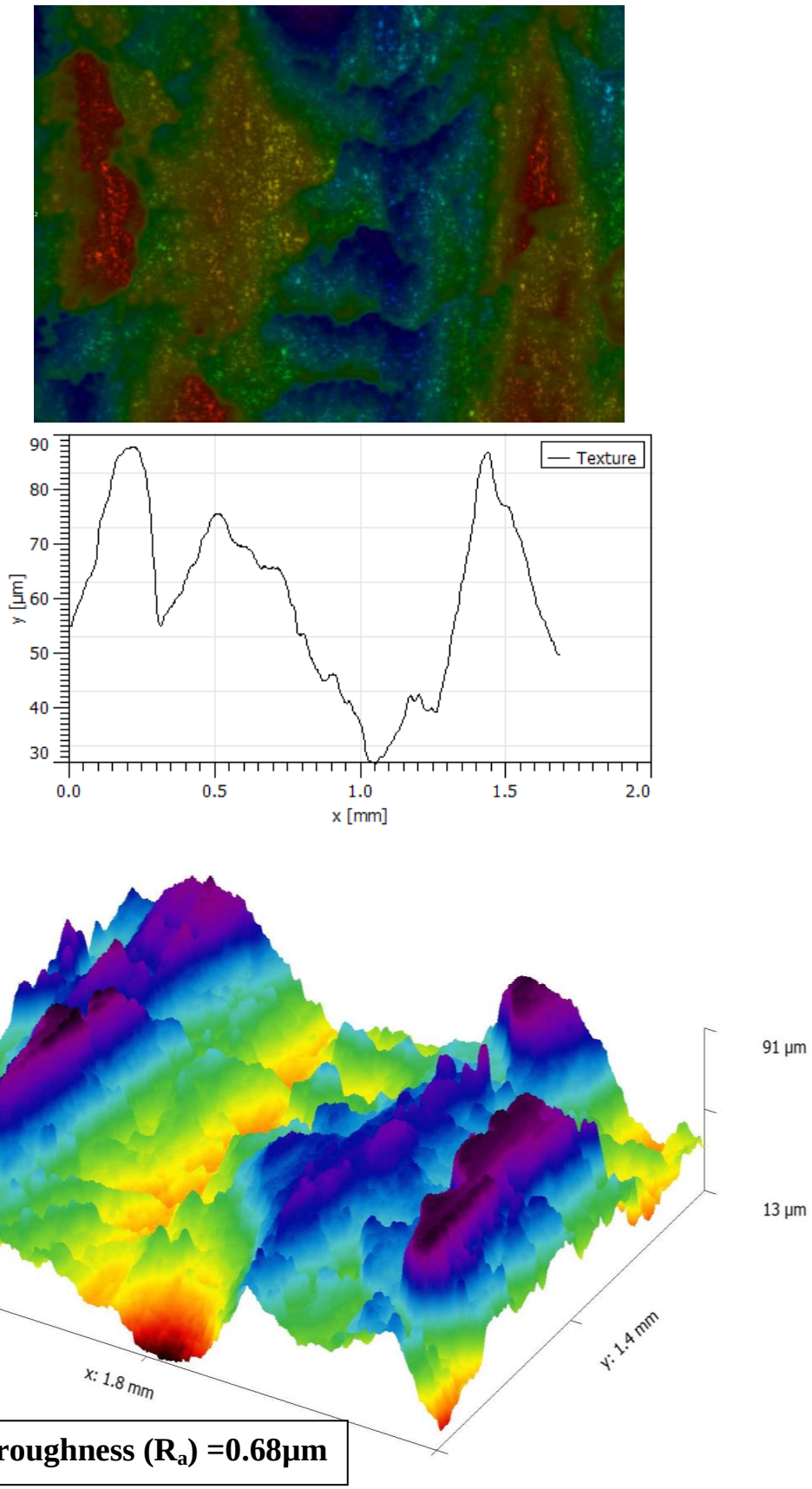

Figure 3.18: Line analysis and 3D profilometer image for the alloy produced by rheocasting with 1200 rpm stirring speed at 30 N load and 5 m/s sliding velocity.

3.4 Conclusions

Al-10Cu alloys were produced by rheocasting at different stirring speeds. The change in microstructure and wear properties were compared with that of metal mould cast alloy. All the rheocast alloys displayed nearly spherical morphology of the primary α – phase whereas metal mould cast sample show fully dendritic microstructure. The primary α - phase is changed from dendritic to nearly spheroidal morphology arsing from stirring action of the melt. The finer grain size of primary α - phase was observed at maximum rotational speed of 1200 rpm. The cumulative volume loss of all alloys increased with increase in load irrespective of the processing method. The coefficient of friction values for rheocast samples were observed to be less than the metal mould cast alloy. The wear rate of metal mould cast alloy rapidly increased beyond 3 m/s sliding velocity. For rheocast alloys, 4 m/s is critical sliding velocity and beyond this wear rate is increased drastically. The microstructural change, particularly, fine grain size and its nearly globular morphology of the primary α-phase could be reason for improvement in wear properties of the rheocast alloys. The coefficient of friction increases with increase in sliding velocity for all the alloys. The value of the coefficient of friction of the alloy produced by rheocasting at 1200 rpm stirring speed was relatively low at all sliding speeds.